Beyond the Gross-Pitaevskii Equation

A Perturbative Approach

Anton Johansson

LUND
UNIVERSITY

Preface

Thesis submitted for the degree *Master in Science in Engineering. Engineering Physics* at the Faculty of Engineering (LTH) at Lund University in June 2021.

Supervisor:	Jakob Bengtsson
Co-supervisor:	Stephanie Reimann
Examiner:	Andrea Idini
Student opponent:	Johan Boström

Abstract

We propose and implement a beyond Gross-Pitaevskii approach based on Many-Body Perturbation theory (MBPT) for the study of Bose-Einstein Condensate (BECs) ground states. Two partitions of the system Hamiltonian are considered. Firstly, a bosonic analogue to Møller-Plesset simply dubbed RSPT, and secondly an approach based on the Epstein-Nesbet partitioning scheme labeled ENPT. We consider one-dimensional BECs and work in the Harmonic Oscillator (HO) basis. Both third order RSPT and ENPT show overall good agreement with Full Configuration Interaction (FCI) in the low-particle number regime for a harmonically trapped BEC. For the same system, fast convergence is also seen towards the GP energy in the mean-field limit, as expected. Moreover, third order ENPT is seen to consistently produce lower ground state energies with better accuracy, compared to RSPT. Finally, we explore more complicated systems. Firstly, a BEC trapped in a double-well potential, where the mean-field ground state exhibits symmetry breaking. For low enough particle counts, when far away from the mean-field limit, we found that third order ENPT applied to a symmetric mean-field state results in lower energies compared to starting from the asymmetric mean-field ground state. Further studies examining the perturbed wave functions are necessary to determine whether or not this ground state is symmetric. Lastly, we study self-bound BEC droplet states, and although our methods are not able to correctly reproduce the characteristic energy minima they do hold promise in the study of self-bound states. Future studies exploring other starting points such as the extended GP equation are proposed.

Acknowledgements

I would like to extend my deepest gratitude towards my supervisor Jakob Bengtsson and co-supervisor Stephanie Reimann, without whom this thesis would neither have been possible nor completed. In addition to fruitful discussions and great feedback, I want to especially thank Jakob Bengtsson for his invaluable help in ensuring the accuracy and correctness of the perturbative calculations. To Stephanie Reimann I want to emphasize how thankful I am for the fantastic input and discussion, but also for the opportunity to undertake this thesis as a part of the many-body quantum mechanics group, in the first place. I also want to specifically thank the group for providing motivation and a wonderful sense of community during these times.

Last but note least, my friends and family. Your unconditional love and support was what made all of this possible to begin with. Everything from the start of my studies in Lund 2016 to the completion of this thesis.

List of abbreviations

NLSE	Non-Linear Schrödinger Equation
GP	Gross-Pitaevskii
BeMF	Best Mean-Field
CI	Configuration Interaction
FCI	Full Configuration Interaction
CISD	Configuration Interaction with Single and Double substitutions
QCISD	Quadratic CISD
CC	Coupled Cluster
PT	Perturbation Theory
MBPT	Many-Body Perturbation Theory
RSPT	Rayleigh-Schrödinger Perturbation Theory
ENPT	Epstein-Nesbet Perturbation Theory
SCF	Self-Consistent Field
HO	Harmonic Oscillator

Contents

Chapter 1

Introduction

This thesis is primarily concerned with the study of perturbation theory based computational methods, applied to finding the ground state energies of non-uniform dilute Bose-Einstein Condensates (BECs). However, before turning to the motivation of this thesis, some background is required.

A BEC refers to the state of matter where a bosonic gas condenses into a single quantum state at ultra-cold temperatures, made possible due to the ability of multiple bosons to reside in the same one-body state (in contrast to fermions). Theoretical predictions on the existence of BECs dates back to papers published in the 1920s by A. Einstein and S. N. Bose, where a statistical model of a non-interacting Bose-gas showed condensation into the ground state at ultra-cold temperatures [1]. Experimental verification followed in 1995 where condensation was achieved in trapped atomic gases of rubidium-87 and sodium [2, 3]. Since then, in addition to atomic gases, condensation has been found in trapped bosonic gases consisting of molecules [4, 5, 6], quasi-particles [7, 8], and photons [9, 10].

Describing interacting many-body systems theoretically is notoriously difficult and the Hamiltonians for such systems are often highly coupled, making analytical approaches unfeasible at the present [11]. Considering a system of N particles labeled by their position $x_1, x_2, \ldots, x_N$ the difficulty arises from the interaction terms $V(x_i, x_j), i \neq j$ in the many-body Hamiltonian which couple the movement of particles x_i and x_j. A common technique for dealing with the coupled nature of the many-body Hamiltonian is the *mean-field* approximation which attempts to describe the interactions of particle x_i with all others in the condensate $\sum_{j=1}^{N} V(x_i, x_j), i \neq j$ by an effective potential $u_{\mathrm{MF}}(x_i)$ [11]. Consequently, the highly coupled many-body Hamiltonian is reduced to the sum of N one-body Hamiltonians, greatly reducing the complexity of the problem [11].

In the mean-field treatment of BECs, assuming all N particles occupy the ground state $|\phi_0\rangle$, one arrives at the one-body Hamiltonian known as the Gross-Pitaevskii (GP) equation [1, 12]. More precisely, this equation is a Non-Linear-Schrödinger Equation (NLSE) describing the multiply occupied one-body state $|\phi_0\rangle$ [1, 12]. Importantly, the GP equation (and modifications thereof) have been successfully applied in describing various properties of trapped weakly interacting dilute BECs, under the assumption that the particle count is large. For instance, the GP equation has not only correctly produced the ground state density of the experimentally verified rubidium-87 BEC [3, 13], but also frequencies of collective excitation modes [14, 15, 16], as well as the formation and dynamics of vortices [17, 18, 19, 20, 21, 22]. Despite this success, with the recent discovery of self-bound BECs through the inclusion of beyond mean-field corrections [23], and its

even more recent experimental verification [24], interest is on the rise for beyond mean-field descriptions. In addition, for larger attractive interaction strengths and certain potentials, a so called Best Mean-Field (BeMF) description that allows for two different one-body states $|\phi_0\rangle, |\phi_1\rangle$ to be occupied have provided lower energies than the GP equation [25]. From the theory of calculus of variations we expect the ground state to be the state that minimizes the energy functional of the system, and as such BeMF sometimes constitutes a better description of the condensate [26].

If we consider a BEC of N particles, how might one go beyond the mean-field description? A common approach is to solve the GP equation in a basis of size M, after which one obtains the GP ground state along with a set of $M-1$ virtual excited one-body states. By then considering various configurations of the N particles in these M states we can arrive at a more accurate description of the BEC ground state. One such method that has seen extensive use over the years in the field of quantum chemistry is Configuration Interaction (CI), where the full BEC ground state is expanded in a basis of these configurations [27]. From this one can construct a matrix representation of the full system Hamiltonian and the ground state energy and expansion coefficients are obtained from the associated eigenvalue problem. If all possible configurations are included in the basis expansion, the method is called Full CI (FCI) and the energies and states obtained are exact in that they are optimal for a given particle count N and set of one-body states [27]. However, the usefulness of FCI is limited to low particle numbers as the matrix sizes and thus computational costs grows too rapidly with increasing N. This problem can partially be remedied, at the cost of accuracy, by considering only a subspace of the configuration space. It is then common to place all particles in the one-body ground state save one or two. The method resulting from this type of truncation is referred to as CI with Single and Double substitutions (CISD) [27]. On the other hand, these approximations are not without drawbacks, and CISD (or any truncated CI method) is not *size-extensive* meaning the energy of the system does not scale linearly with N as one would expect [27]. There is also the closely related property of *size-consistency* which concerns the consistency of the method across chemical reactions, for instance for the dissociation $AB \to A + B$, the numerical method is size-consistent if it the energy of AB is the same as the combined energy of A and B [27]; Size-consistency will not be a problem in this thesis as no such systems are considered. Note, there are many variants of CI and only a fraction of them were brought up here.

The use of truncated CI methods eventually faded in favor of truncations of more efficient methods such as Many-Body Perturbation theory (MBPT) and later Coupled Cluster (CC). Both MBPT and CC, including their truncated variants, are size-extensive [27, 28]. In the last decade however, interest in truncated MBPT based methods is again on the rise due to its improved scaling with particle count and often better time-complexity, compared to CC. Additionally the MBPT methods (as most of the methods mentioned) exist in many variations and are often tailored to the specific problem at hand. For instance, in the study of open-shell nuclei in nuclear structure theory a particular Bogoliubov based MBPT method has recently shown much promise, reproducing the results from non-perturbative methods such as CI and CC at a fraction of the computation time [29, 30, 31]. Similarly, in the study of electronic systems the common time-independent second order Møller-Plesset perturbation theory was in the early 2010s extended to use optimized virtual orbitals, resulting in both increased accuracy of computed molecular properties but also making the method more competitive compared to non-perturbative approaches [32, 33]. This method was recently made time-dependent and applied in the

numerical study of atoms in strong laser fields, specifically high harmonic generation, with great results [34].

The goal of this thesis may then be stated as: Firstly, to go beyond the mean-field description via MBPT, where the virtual one-body states obtained in solving the GP equation self-consistently will be incorporated to include higher order corrections to ground state energy; Secondly, to verify our MBPT approach against FCI and the GP equation in their respect regimes, where they are accurate; Lastly, to study more complicated systems where the normal GP approach is insufficient and FCI is computationally infeasible. Here we consider a one-component BEC in a double well where the GP equation shows symmetry breaking [35], and a two-component self-bound BEC which is not able to be described via the GP equation [23].

Motivations for this thesis are manyfold: Firstly, the implementation of such a method serves as a stepping stone in implementing more involved bosonic beyond mean-field methods such as Quadratic CISD (QCISD), correcting the size-inconsistency of CISD [36], CC, and possibly more complicated MBPT variants [27]; Secondly, it allows for the efficient and novel theoretical study of BECs in the intermediate particle number regime where not much is known for larger interaction strengths. We restrict ourselves to the study of one-dimensional BECs with contact interaction as a suitable starting point.

Let us now briefly outline the rest of this thesis. In chapter 2 the prerequisite knowledge in many-body theory is covered, it also presents the mean-field approximation along with the GP and BeMF equations. Additionally, this chapter covers the Self-Consistent Field (SCF) method and the used approaches to MBPT. Chapter 3 contains all derivations pertaining to the perturbative energy shifts of the GP ground state. Moving on, the main results of this thesis is presented in Chapter 4 where a one-component BEC in a harmonic trap is firstly studied to determine the convergence behavior of the perturbative methods. Followed by the study of a one-component BEC in a double well and a two-component self-bound BEC. Lastly, the main results are summarized in Chapter 5 and an outlook is provided in Chapter 6.

Chapter 2

Theoretical background

This chapter starts out with an overview of many-body theory using second quantization in Sec. 2.1, particularly as applied to systems with contact interaction. Next, the mean-field approximation is presented in Sec. 2.2 along with its use in deriving the one- and two-component GP and one-component BeMF equations. In order to solve these non-linear one-body equations, the numerical SCF method is put forth in Sec. 2.3 along with techniques to aid in convergence. Finally the necessary foundations in MBPT are provided in Sec. 2.4 where two different approaches to Hamiltonian partitioning are considered.

2.1 Many-body theory with contact interaction

As a suitable starting point, consider a particle of mass m in an external potential $\hat{u}$. The Hamiltonian of this system is then given by

$$\hat{h} = \frac{\hat{p}^2}{2m} + \hat{u}, \tag{2.1}$$

where $\hat{p}$ is the momentum operator [37]. Further, the stationary energy spectrum $\{\epsilon_n\}$ and eigenstates $\{|\phi_n\rangle\}$ of $\hat{h}$ are given by the one-body Schrödinger equation

$$\hat{h}|\phi_n\rangle = \epsilon_n|\phi_n\rangle, \quad |\phi_n\rangle \in \mathcal{H}, \tag{2.2}$$

where solutions $|\phi_n\rangle$ live in the one-body Hilbert space $\mathcal{H}$. From this point onwards all equations will be presented in natural units, setting $\hbar = c = m = 1$.

We will also work in the position basis where $\phi_n(x) = \langle x|\phi_n\rangle$, and $\hat{h}(x) = -\frac{1}{2}\frac{\partial^2}{\partial x^2} + u(x)$. A system of N non-interacting bosons labeled by their position $x_1, x_2, \ldots, x_N$ may be described by the many-body Hamiltonian [11]

$$\hat{H} = \sum_{i=1}^{N} \hat{h}(x_i). \tag{2.3}$$

However, if inter-particle interactions are to be included, terms linking different x_i will have to be added. The most basic form of which is *contact interaction*, which between particles of sufficiently low energies and momenta takes the form a of a delta function $g\delta(x_i - x_j)$ [12]. Here $g = 4\pi\hbar^2 a/m$ refers to the interaction strength consisting of the scattering length a and particle mass m [12]. This approximation is reasonable as BECs

are dilute gases at ultra-cold temperatures [12].

Including contact interactions, the Hamiltonian in Eq. (2.3) now becomes

$$\hat{H} = \sum_{i=1}^{N} \hat{h}_i(x_i) + g \sum_{i<j}^{N} \delta(x_i - x_j), \tag{2.4}$$

where $\sum_{i<j}^{N}$ denotes a double sum over indices $i, j \in [1, N]$ such that $i < j$. This type of sum is required to avoid double counting interactions. Working with the Hamiltonian in Eq. (2.4) is easiest in the formalism of second quantization (see Appendix A for an overview) where it reads

$$\hat{H} = \sum_{ij} h_{ij} \hat{a}_i^\dagger \hat{a}_j + \frac{1}{2} g \sum_{ijkl} v_{ijkl} \hat{a}_i^\dagger \hat{a}_j^\dagger \hat{a}_l \hat{a}_k, \tag{2.5}$$

with $h_{ij} = \int \mathrm{d}x\, \phi_i^*(x) \hat{h}(x) \phi_j(x)$ and $v_{ijkl} = \int \mathrm{d}x\, \phi_i^*(x) \phi_j^*(x) \phi_k(x) \phi_l(x)$. The sums above $\sum_{ij}$ and $\sum_{ijkl}$ run over all one-body states. Note also that the integrals have the implicit bounds $(-\infty, \infty)$. In the second quantization formalism, many-body states are elements of the symmetric *Fock space* $\mathcal{F}_s(\mathcal{H})$ over the one-body Hilbert space $\mathcal{H}$ introduced earlier. Elements of this space are symmetric with respect to particle interchange. As such, this space contains all possible bosonic many-body states constructed from elements of $\mathcal{H}$. It is common to reference elements of the Fock space using the occupation number notation. In this notation, a many-body state of N particles in M different orthogonal one-body states is labeled by $|n_0, n_1, \ldots, n_{M-1}\rangle \in \mathcal{F}_s(\mathcal{H})$ which corresponds to n_0 particles in $|\phi_0\rangle$, n_1 in $|\phi_1\rangle$, and so on. Additionally the inner product between two many-body states is only non-zero when they both contain the same one-body states with the same occupancies.

Including another species of bosons and making sure that the particle count of each species is conserved, we arrive at a system consisting of two chemically independent components, one component per species. Each component may be labeled A, B with their respective particle counts N_A, N_B, and intra- and inter-component interactions strengths g_{AA}, g_{BB} and g_{AB} respectively. The Hamiltonian of the two-component system may now be constructed from Hamiltonians $\hat{H}_A$ and $\hat{H}_B$ taking the form of Eq. (2.4) covering the intra-component interactions, along with a separate term accounting for inter-component interactions. This yields

$$\begin{aligned}
\hat{H} &= \hat{H}_A + \hat{H}_B + \sum_{i=1}^{N_A} \sum_{j=1}^{N_B} g_{AB} \delta(x_{A_i} - x_{B_j}) \\
&= \left(\sum_{i=1}^{N_A} \hat{h}_A(x_{A_i}) + \sum_{i<j}^{N_A} g_{AA} \delta(x_{A_i} - x_{A_j}) \right) \\
&\quad + \left(\sum_{i=1}^{N_B} \hat{h}_B(x_{B_i}) + \sum_{i<j}^{N_B} g_{BB} \delta(x_{B_i} - x_{B_j}) \right) \\
&\quad + \sum_{i=1}^{N_A} \sum_{j=1}^{N_B} g_{AB} \delta(x_{A_i} - x_{B_j}).
\end{aligned} \tag{2.6}$$

Note the relabeling of indices such as $i \to A_i$ to better separate the components. Express-

ing Eq. (2.6) in second quantization now results in

$$\begin{aligned}\hat{H} = &\sum_{ij} h_{ij}^{(A)} \hat{a}_{A_i}^\dagger \hat{a}_{A_j} + \frac{1}{2} g_{AA} \sum_{ijkl} v_{ijkl}^{(AA)} \hat{a}_{A_i}^\dagger \hat{a}_{A_j}^\dagger \hat{a}_{A_l} \hat{a}_{A_k} \\ &+ \sum_{ij} h_{ij}^{(B)} \hat{a}_{B_i}^\dagger \hat{a}_{B_j} + \frac{1}{2} g_{BB} \sum_{ijkl} v_{ijkl}^{(BB)} \hat{a}_{B_i}^\dagger \hat{a}_{B_j}^\dagger \hat{a}_{B_l} \hat{a}_{B_k} \\ &+ g_{AB} \sum_{ijkl} v_{ijkl}^{(AB)} \hat{a}_{A_i}^\dagger \hat{a}_{B_j}^\dagger \hat{a}_{B_l} \hat{a}_{A_k},\end{aligned} \tag{2.7}$$

where (with "P" and "Q" as placeholders),

$$h_{ij}^{(P)} = \int \mathrm{d}x\, \phi_{P_i}^*(x) \hat{h}_P(x) \phi_{P_j}(x), \tag{2.8}$$

and

$$v_{ijkl}^{(PQ)} = \int \mathrm{d}x\, \phi_{P_i}^*(x) \phi_{Q_j}^*(x) \phi_{P_k}(x) \phi_{Q_l}(x). \tag{2.9}$$

Furthermore, the space of many-body two-component states is the combination of the one-component Fock spaces $\mathcal{F}_s^{(AB)}(\mathcal{H}) := \mathcal{F}_s^{(A)}(\mathcal{H}) \otimes \mathcal{F}_s^{(B)}(\mathcal{H})$ where "$\otimes$" denotes the tensor product. Elements of this space take the form $|n_{A_0}, n_{A_1}, \ldots\rangle \otimes |n_{B_0}, n_{B_1}, \ldots\rangle \in \mathcal{F}_s^{(AB)}(\mathcal{H})$ and contains n_{A_0} particles in $|\phi_{A_0}\rangle$, n_{B_0} in $|\phi_{B_0}\rangle$ and so on. Similarly to the one-component case, the inner product in this space is only non-zero between many-body states containing the same components, one-body states and occupancies of those states. More information regarding the mathematical construction of the Fock spaces is provided in Appendix A.

Note, that in the strictest sense the one- and two-component Hamiltonians presented in Eq. (2.5) and (2.7) are not actually Hamiltonians as they have a non-linear dependence on the one-body states $\{|\phi_{P_i}\rangle\}$. Rather they should be considered as Hamiltonian-generators which for a given set $\{|\phi_{P_i}\rangle\}$ produces a linear Hamiltonian. We will however only be dealing with these Hamiltonian-generators in the context of a given set of one-body states, meaning the distinction is not necessary.

All in all, the stationary bosonic many-body problem can be phrased as the time-independent many-body Schrödinger equation

$$\hat{H}|\Psi_n\rangle = E_n|\Psi_n\rangle, \quad |\Psi_n\rangle \in \mathcal{F}_s(\mathcal{H}), \tag{2.10}$$

where solutions $|\Psi_n\rangle$ are sought after in the bosonic Fock space $\mathcal{F}_s(\mathcal{H})$, instead of the usual one-body Hilbert space $\mathcal{H}$ in the one-body Schrödinger equation (2.2).

Notation-wise, uppercase symbols will refer to many-body quantities. For instance, the many-body state $|\Psi_n\rangle$, Hamiltonian $\hat{H}$, and eigenvalue E_n. Similarly, lowercase symbols refer to one-body quantities, such as the one-body state $|\phi_n\rangle$, Hamiltonian $\hat{h}$, and eigenvalue ϵ_n.

2.2 The mean-field approximation

As previously mentioned, the mean-field approximation is a powerful tool in dealing with highly coupled interacting systems such as the full many-body one- and two-component Hamiltonians $\hat{H}$ given by Eq. (2.4) and (2.6). By assuming all inter-particle interactions

may be approximated by an effective mean-field potential $\hat{u}_{\mathrm{MF}}(x)$, the full one-component Hamiltonian $\hat{H}$ of a N particle system can be estimated by

$$\hat{H}_{\mathrm{MF}} = \sum_{i=1}^{N} (\hat{h}(x_i) + \hat{u}_{\mathrm{MF}}(x_i)), \tag{2.11}$$

where $\hat{h}(x)$ is the linear Hamiltonian in Eq. (2.1) [11]. The problem has now been reduced to studying N identical one-body Hamiltonians, however the problem of finding $\hat{u}_{\mathrm{MF}}(x)$ still remains. Fortunately, for a given many-body state $|\Psi\rangle \in \mathcal{F}_s(\mathcal{H})$ the optimal mean-field Hamiltonian

$$\hat{h}_{\mathrm{MF}} = \hat{h} + \hat{u}_{\mathrm{MF}} \tag{2.12}$$

can be found by minimizing the energy functional $E = \langle\Psi|\hat{H}|\Psi\rangle$ with respect to the one-body states in $|\Psi\rangle$ [11]. A few such mean-field Hamiltonians resulting from different many-body states $|\Psi\rangle$ will be presented in the following sections.

2.2.1 One- and two-component Gross-Pitaevskii equations

The derivation of the one- and two-component GP equations presented here uses a variational approach, another common method is to use field operators and the Bogoliubov approximation, see Ref. [1] for more information on the topic.

The full energy of a N particle many-body state $|\Psi\rangle \in \mathcal{F}_s(\mathcal{H})$ in a one-component system with contact interaction is given by $E = \langle\Psi|\hat{H}|\Psi\rangle$, where $\hat{H}$ is given by Eq. (2.5). Clearly, E depends on the choice of $|\Psi\rangle$, and in a BEC at ultra-cold temperatures it is reasonable to assume that only the lowest energy one-body state $|\phi_0\rangle$ is occupied. Therefore $|\Psi\rangle = |N, 0, \ldots\rangle$ and the energy functional E becomes

$$E[\phi_0] = \langle\Psi|\hat{H}|\Psi\rangle = N \int \mathrm{d}x \left(\phi_0^*(x)\hat{h}(x)\phi_0(x) + \frac{1}{2}g(N-1)|\phi_0(x)|^4 \right). \tag{2.13}$$

Minimization of Eq. (2.13) with respect to $\phi_0(x)$, using the Lagrange multiplier μ_0, we find the one-component GP equation

$$\left(\hat{h}(x) + g(N-1)|\phi_0(x)|^2\right)\phi_0(x) = \mu_0\phi_0(x), \tag{2.14}$$

as an equivalency to the Euler-Lagrange equation [12, 26]. Equation (2.14) must be satisfied for $\phi_0(x)$ to be an extremal of the energy functional [12, 26]. Note, this form of the GP equation differs from that commonly presented in the literature, where the interaction term is given by $gN|\phi_0(x)|^2$. Usually, Eq. (2.14) is shown in terms of the order parameter $\phi_{\mathrm{ord}}(x) = \sqrt{N}\phi_0(x)$ and $N \gg 1$ is assumed such that $g(N-1) \approx gN$. The order parameter also takes degenerate ground states into account which we do not consider here. Furthermore, $\phi_0(x)$ satisfying Eq. (2.14) does not guarantee that it minimizes $E[\phi_0]$, but only that it is an extremal of $E[\phi_0]$, and relying on the theory of variational calculus to ensure a minimum of $E[\phi_0]$ is possible only in the special cases where Eq. (2.14) is analytically solvable [26]. Therefore, it is often necessary to try multiple $\phi_0(x)$ to ensure a minimum. Additionally, the eigenvalues μ_0 in Eq. (2.14) are not energies as one might expect, but chemical potentials as they can be shown to satisfy $E[\phi_0, N] - E[\phi_0, N-1] = \mu_0$ (treating Eq. (2.13) as a function of N) [12].

Similarly to the one-component case, the ground state of a BEC with components A and B can be described by a many-body state $|\Psi\rangle \in \mathcal{F}_s^{(AB)}(\mathcal{H})$. Assuming N_A particles in the ground state $|\phi_{A_0}\rangle$ of component A and N_B in the ground state $|\phi_{B_0}\rangle$ of B, then the BEC ground state becomes $|\Psi\rangle = |N_A, 0, \ldots\rangle \otimes |N_B, 0, \ldots\rangle$. Consequently the energy functional $E = \langle\Psi|\hat{H}|\Psi\rangle$ can be calculated as

$$\begin{aligned} E[\phi_{A_0}, \phi_{B_0}] = N_A \int \mathrm{d}x \left(\phi_{A_0}^*(x)\hat{h}(x)\phi_{A_0}(x) + \frac{1}{2} g_{AA}(N_A - 1)|\phi_{A_0}(x)|^4 \right) \\ + N_B \int \mathrm{d}x \left(\phi_{B_0}^*(x)\hat{h}(x)\phi_{B_0}(x) + \frac{1}{2} g_{BB}(N_B - 1)|\phi_{B_0}(x)|^4 \right) \\ + g_{AB} N_A N_B \int \mathrm{d}x \, |\phi_{A_0}(x)|^2 |\phi_{B_0}(x)|^2, \end{aligned} \tag{2.15}$$

when using the two-component Hamiltonian Eq. (2.7) in second quantization. Minimization of Eq. (2.15) with respect to $\phi_{A_0}(x)$ and $\phi_{B_0}(x)$, using Lagrange multipliers μ_{A_0} and μ_{B_0}, then results in the two-component GP equation

$$\begin{cases} \left(\hat{h}(x) + g_{AA}(N_A - 1)|\phi_{A_0}(x)|^2 + g_{AB} N_B |\phi_{B_0}(x)|^2 \right) \phi_{A_0}(x) = \mu_{A_0} \phi_{A_0}(x) \\ \left(\hat{h}(x) + g_{BB}(N_B - 1)|\phi_{B_0}(x)|^2 + g_{AB} N_A |\phi_{A_0}(x)|^2 \right) \phi_{B_0}(x) = \mu_{B_0} \phi_{B_0}(x) \end{cases}, \tag{2.16}$$

as a pair of coupled eigenvalue equations.

Lastly, a few words have to be said about the validity of the GP equations presented. These mean-field equations are known to be valid in the *mean-field limit* where the interaction strength scales as $g = 1/(N-1)$ as $N \to \infty$, keeping the non-linear parameter $\lambda = g(N-1)$ constant [38]. In this limit it has been shown that the mean-field energy $E[\phi_0]$ correctly approaches the minimum energy eigenvalue of $\hat{H}$ [38].

2.2.2 One-component best mean-field equation

By extending the mean-field description to allow for two occupied one-body states a lower mean-field energy may be achieved - specifically in the case of strongly attractive interparticle interactions [25]. However, consider a condensate in a trap with $N = n_0 + n_1$ particles where n_0 reside in $|\phi_0\rangle$ and n_1 in $|\phi_1\rangle$ corresponding to the many-body state $|\Psi\rangle = |n_0, n_1, 0, \ldots\rangle \in \mathcal{F}_s(\mathcal{H})$. Then theoretically, so called *fragmentation* can occur where both $|\phi_0\rangle$ and $|\phi_1\rangle$ have large occupations n_0 and n_1, and the condensate has effectively split in two, each with ground state $|\phi_0\rangle$ and $|\phi_1\rangle$ respectively [1, 39]. Fragmentation is something to be mindful of, since it is possible in this model [25, 40].

Proceeding with the derivation of the mean-field equations, using the $|\Psi\rangle$ above, the energy functional reads

$$\begin{aligned} E[\phi_0, \phi_1, n_0, n_1] = n_0 \int \mathrm{d}x \left(\phi_0^*(x)\hat{h}(x)\phi_0(x) + \frac{1}{2} g(n_0 - 1)|\phi_0(x)|^4 \right) \\ + n_1 \int \mathrm{d}x \left(\phi_1^*(x)\hat{h}(x)\phi_1(x) + \frac{1}{2} g(n_1 - 1)|\phi_1(x)|^4 \right) \\ + 2g n_0 n_1 \int \mathrm{d}x \, |\phi_0(x)|^2 |\phi_1(x)|^2, \end{aligned} \tag{2.17}$$

which is to be minimized with respect to $\phi_0(x)$, $\phi_1(x)$, n_0 and n_1 [25]. Note that the BeMF energy functional above looks remarkably similar to the two-component GP energy functional in Eq. (2.15), the major difference however is in the factor 2 in the last term. This factor 2 is not present in the two-component case where we require the conservation of particle counts in each component, cutting the number of possible interactions in half. From the energy functional in Eq. (2.17) it also becomes clear that fragmentation is not a favorable process. This is because we are dealing with attractive interactions $g < 0$ and as such the exchange integral in Eq. (2.17) is minimized when the overlap between $|\phi_0(x)|^2$ and $|\phi_1(x)|^2$ is at a maximum.

Next, carrying out the minimization with respect to $\phi_0(x)$ and $\phi_1(x)$, using Lagrange multipliers $\mu_{00}, \mu_{01}, \mu_{11}, \mu_{10}$, yields the system of equations

$$\begin{cases} \left(\hat{h}(x) + g(n_0 - 1)|\phi_0(x)|^2 + 2gn_1|\phi_1(x)|^2\right)\phi_0(x) = \mu_{00}\phi_0(x) + \mu_{01}\phi_1(x) \\ \left(\hat{h}(x) + g(n_1 - 1)|\phi_1(x)|^2 + 2gn_0|\phi_0(x)|^2\right)\phi_1(x) = \mu_{10}\phi_0(x) + \mu_{11}\phi_1(x) \end{cases}, \tag{2.18}$$

which notably are not eigenvalue equations [25]. However, at optimal n_0 and n_1 it can be shown what $\mu = \mu_{00} = \mu_{11}$, and further assuming $n_0 \gg 1, n_1 \gg 1$, introducing the new orbitals

$$\begin{cases} \psi_0(x) = \sqrt{\frac{n_0}{N}}\phi_0(x) + \sqrt{\frac{n_1}{N}}\phi_1(x) \\ \psi_1(x) = \sqrt{\frac{n_1}{N}}\phi_1(x) - \sqrt{\frac{n_0}{N}}\phi_0(x) \end{cases}, \tag{2.19}$$

transforms Eq. (2.18) to an eigenvalue problem more akin to the two-component GP equation (2.16)

$$\begin{cases} \left(\hat{h} + \frac{3}{4}g(N-1)|\psi_0(x)|^2 + \frac{1}{4}g(N-1)|\psi_1(x)|^2\right)\psi_0(x) = (\mu + \bar{\mu})\psi_0(x) \\ \left(\hat{h} + \frac{3}{4}g(N-1)|\psi_1(x)|^2 + \frac{1}{4}g(N-1)|\psi_0(x)|^2\right)\psi_1(x) = (\mu - \bar{\mu})\psi_1(x) \end{cases} \tag{2.20}$$

where $\bar{\mu} = \sqrt{n_0/n_1}\mu_{01} = \sqrt{n_1/n_0}\mu_{10}$ [25]. Additionally $|\psi_0\rangle$ and $|\psi_1\rangle$ are non-orthogonal with the inner product $\langle\psi_0|\psi_1\rangle = (n_1 - n_0)/N$ which may be used to retrieve the optimal occupations n_0 and n_1.

Importantly, even though Eq. (2.20) was derived on the premise that $n_0 \gg 1, n_1 \gg 1$ and thus $N = n_0 + n_1 \gg 1$, it is not required to solve for the correct states $|\psi_0\rangle$ and $|\psi_1\rangle$. The problem can be rescaled, for instance if $\lambda = g(N-1) = 1$ then $N = 1000, g = 1/999$ will yield the same solution as $N = 4, g = 1/3$ despite $N \gg 1$ not being satisfied. Furthermore, the size of N is only important when solving $\langle\psi_0|\psi_1\rangle = (n_1 - n_0)/N$ for the optimal n_0 and n_1 and when computing the energy $E[\phi_0, \phi_1, n_0, n_1]$, where a large N will yield more accurate results. However if all we are interested in are the fractional occupations n_0/N and n_1/N, then the size of N is not an issue. Note here that if $n_0 = 0$ or $n_1 = 0$ then $\psi_0(x) = \psi_1(x)$, and $\bar{\mu} = 0$ and Eq. (2.20) reproduces the one-component GP equation.

2.3 Solving non-linear Schrödinger-like equations via the self-consistent field method

The goal of this section is to present the Self-Consistent Field (SCF) method as an approach to solve one-body eigenvalue problems with a non-linear dependence on the one-body states, such as those posed by the GP and BeMF equations (2.14), (2.16) and (2.20). The method itself has proved an invaluable tool in solving these eigenvalue problems ever since its first application in the 1950s where it allowed for the numerical study of atomic and molecular orbitals [41, 42].

We are interested in finding eigenstates of the mean-field Hamiltonian $\hat{h}_{\mathrm{MF}} = \hat{h} + \hat{u}_{\mathrm{MF}}$, where $\hat{h}$ is given by Eq. (2.1) and $\hat{u}_{\mathrm{MF}}$ is the mean-field effective potential which depends on the sought-after eigenstate $|\phi\rangle$. Remember here that $\hat{h}_{\mathrm{MF}}$ is actually a Hamiltonian-generator with non-linear dependence on the eigenstate $|\phi\rangle$. However for a given $|\phi\rangle$ the generated Hamiltonian is linear. The SCF algorithm is summarized in Fig. 2.1 and steps **(1-4)** will be referenced in following explanation, note steps **(2.a, 3.a)** are not part of the core algorithm and will be discussed shortly. To find the solution $|\phi\rangle$ that satisfies $\hat{h}_{\mathrm{MF}}|\phi\rangle = \mu|\phi\rangle$ the SCF method starts from an initial guess $|\phi^{(0)}\rangle$ (step **(1)**) and assumes $\hat{h}_{\mathrm{MF}}$ acts as a contraction map. The state $|\phi\rangle$ can then be approximated through the process of fixed point iteration. Concretely, this means using $|\phi^{(0)}\rangle$ to construct the Hamiltonian $\hat{h}^{(0)}_{\mathrm{MF}}$ (step **(2)**) and then pick an eigenstate $|\phi^{(1)}\rangle$ of this Hamiltonian as a starting point of the next iteration (steps **(3, 4)**). The choice of eigenstate depends on the desired qualities of the final eigenstate. For instance, choosing $|\phi^{(n+1)}\rangle$ as the eigenstate of $\hat{h}^{(n)}_{\mathrm{MF}}$ with lowest eigenvalue, as we do in this thesis, is great when looking for the ground state of $\hat{h}_{\mathrm{MF}}$. If on the other hand, one is interested in excited states of $\hat{h}_{\mathrm{MF}}$, the eigenstate $|\phi^{(n+1)}\rangle$ of $\hat{h}^{(n)}_{\mathrm{MF}}$ that maximises the overlap $\langle\phi^{(n+1)}|\phi^{(n)}\rangle$ is commonly chosen [43]. Iteration is thus carried out according to the recursive scheme

$$\hat{h}^{(n)}_{\mathrm{MF}}|\phi^{(n+1)}\rangle = \mu^{(n+1)}|\phi^{(n+1)}\rangle \tag{2.21}$$

until convergence is achieved with respect to some criterion, commonly measured in terms of the eigenstates $|\phi^{(n)}\rangle$ or eigenvalues $\mu^{(n)}$.

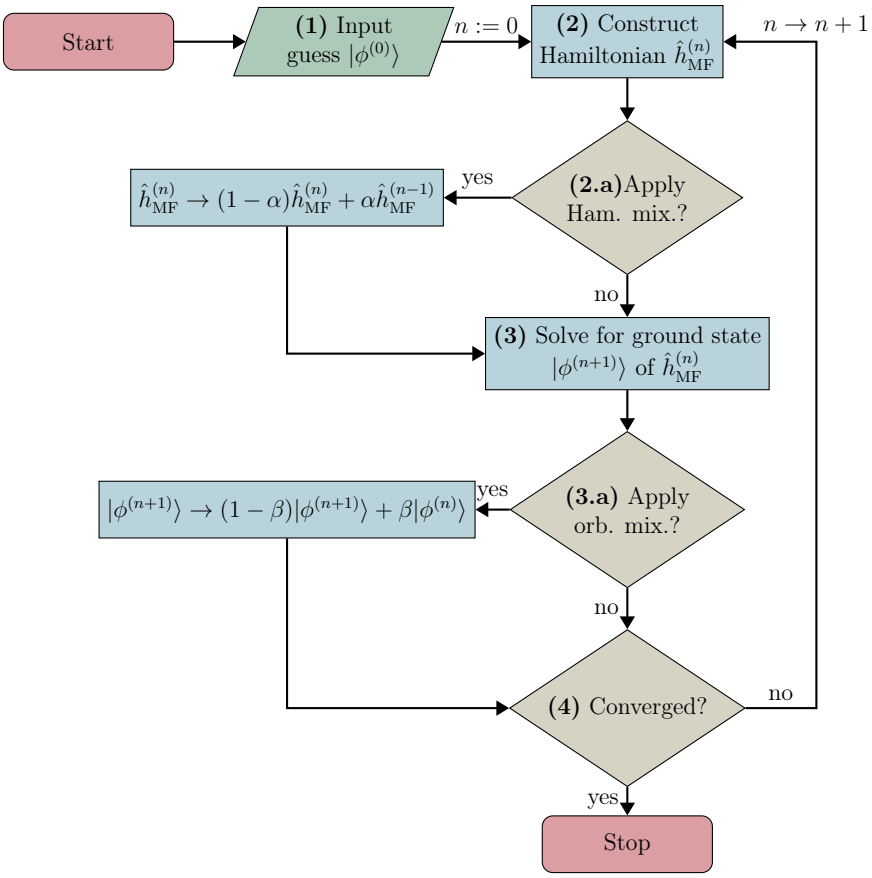

Figure 2.1: Schematic representation of the SCF method, including Hamiltonian and orbital mixing.

Practically, SCF encounters problems of slow convergence and sometimes stability issues such as getting stuck oscillating between two or more states [44]. Methods attempting to rectify these problems are plentiful and appear in most Hartree-Fock based quantum chemistry software packages. One of the most effective remedies that also applies to bosonic systems is *Hamiltonian mixing* (step **(2.a)**) where the Hamiltonian of the $(n+1)$:th iteration is refined by taking the weighted average with n:th Hamiltonian, that is

$$\hat{h}^{(n+1)}_{\mathrm{MF}} \to (1-\alpha)\hat{h}^{(n+1)}_{\mathrm{MF}} + \alpha\hat{h}^{(n)}_{\mathrm{MF}}, \tag{2.22}$$

where $\alpha \in [0, 1)$ is the mixing parameter [44]. A similar approach is *orbital mixing* (step **(3.a)**) where the eigenstates are mixed according to the same scheme

$$|\phi^{(n+1)}\rangle \to (1-\beta)|\phi^{(n+1)}\rangle + \beta|\phi^{(n)}\rangle, \tag{2.23}$$

with the mixing parameter $\beta \in [0, 1)$ [44]. Note that the extension to two-component GP or BeMF is straight forward.

Finally, how does one go about finding the eigenstates of $\hat{h}^{(n)}_{\mathrm{MF}}$? Practically, $\hat{h}^{(n)}_{\mathrm{MF}}$ is expressed as a finite-dimensional matrix $\boldsymbol{h}^{(n)}_{\mathrm{MF}}$ using either a basis- or grid-based approach. Grid based methods rely on either finite difference schemes or spectral methods to compute the spatial derivatives in $\hat{h}^{(n)}_{\mathrm{MF}}$. Finite difference schemes are accurate assuming very fine grids, but result in large matrices to diagonalize every iteration [45]. On the other

hand, spectral methods gets away with better accuracy for coarser grids and thus smaller matrices, however this is not necessarily the case for non-periodic problems [45]. Using basis sets, which is the favored approach in this thesis, allows for easy computation of derivatives resulting in small matrices. This however requires the choice of an appropriate set of basis functions for the problem at hand to get accurate results.

2.4 Many-body perturbation theory

2.4.1 Rayleigh-Schrödinger perturbation theory

Rayleigh-Schrödinger Perturbation Theory (RSPT) arose as a way to approach the time-independent Schrödinger equation (2.2) for complicated Hamiltonians which makes the problem analytically intractable [11, 37]. We consider the many-body Schrödinger equation (2.10) for a Hamiltonian partitionable as

$$\hat{H} = \hat{H}_0 + \lambda \hat{V}, \qquad \lambda \in \mathbb{R}, \tag{2.24}$$

where eigenstates $\{|\Psi_n^{(0)}\rangle\}$ of $\hat{H}_0|\Psi_n^{(0)}\rangle = E_n^{(0)}|\Psi_n^{(0)}\rangle$ are known [11, 37]. Here $\hat{H}_0$ commonly denotes the unperturbed Hamiltonian whilst $\hat{V}$ is the perturbation whose strength is tuned by the real parameter λ.

The goal is to approximate the eigenstates $\{|\Psi_n\rangle\}$ and eigenvalues $\{E_n\}$ of the full Hamiltonian in Eq. (2.24) in terms of the known unperturbed $\{|\Psi_n^{(0)}\rangle\}$ and $\{E_n^{(0)}\}$. The full energy of the state $|\Psi_n\rangle$ may be written as $E_n = E_n^{(0)} + \Delta E_n$, where $\Delta E_n = E_n - E_n^{(0)}$ is the energy shift incurred from the presence of the perturbation $\hat{V}$. Next, the energy shift ΔE_n is expanded in a power series about the perturbation strength λ giving

$$\Delta E_n = \lambda \Delta E_n^{(1)} + \lambda^2 \Delta E_n^{(2)} + \lambda^3 \Delta E_n^{(3)} + \dots \tag{2.25}$$

where the first-, second-, and third order perturbation to the energy, $\Delta E_n^{(1)}, \Delta E_n^{(2)}$, and $\Delta E_n^{(3)}$ respectively can be shown to be (see Refs. [11, 37] for a detailed derivation)

$$\Delta E_n^{(1)} = \langle \Psi_n^{(0)} | \hat{V} | \Psi_n^{(0)} \rangle, \tag{2.26}$$

$$\Delta E_n^{(2)} = \sum_{k \neq n}^{\infty} \frac{|\langle \Psi_k^{(0)} | \hat{V} | \Psi_n^{(0)} \rangle|^2}{E_n^{(0)} - E_k^{(0)}}, \tag{2.27}$$

$$\begin{aligned} \Delta E_n^{(3)} = &\sum_{k \neq n}^{\infty} \sum_{l \neq n}^{\infty} \frac{\langle \Psi_n^{(0)} | \hat{V} | \Psi_l^{(0)} \rangle \langle \Psi_l^{(0)} | \hat{V} | \Psi_k^{(0)} \rangle \langle \Psi_k^{(0)} | \hat{V} | \Psi_n^{(0)} \rangle}{(E_n^{(0)} - E_k^{(0)})(E_n^{(0)} - E_l^{(0)})} \\ &- \langle \Psi_n^{(0)} | \hat{V} | \Psi_n^{(0)} \rangle \sum_{k \neq n}^{\infty} \frac{|\langle \Psi_k^{(0)} | \hat{V} | \Psi_n^{(0)} \rangle|^2}{(E_n^{(0)} - E_k^{(0)})^2}. \end{aligned} \tag{2.28}$$

Importantly, for the energy shifts to be meaningful, the infinite sums above must converge meaning the matrix elements $\langle \cdot | \hat{V} | \cdot \rangle$ must be small and the unperturbed state with energy $E_n^{(0)}$ above must be non-degenerate [37].

2.4.2 Epstein-Nesbet partitioning

Another approach to perturbation theory emanating from quantum chemistry, is that of Epstein and Nesbet [46, 47], where the full Hamiltonian Eq. (2.24) in RSPT is partitioned differently. This approach will be referred to as Epstein-Nesbet Perturbation Theory (ENPT). Note that the Fock space $\mathcal{F}_s(\mathcal{H})$ which the unperturbed many-body states $\{|\Psi_n^{(0)}\rangle\}$ inhabits is complete and $|\Psi_n^{(0)}\rangle$ is a basis in this space. Consequently, $1 = \sum_k^\infty |\Psi_k^{(0)}\rangle\langle\Psi_k^{(0)}|$, where $|\Psi_k^{(0)}\rangle \in \mathcal{F}_s(\mathcal{H})$, and the Hamiltonian $\hat{H}$ can represented as

$$\hat{H} = \sum_{k,k'}^{\infty} |\Psi_k^{(0)}\rangle\langle\Psi_k^{(0)}|\hat{H}|\Psi_{k'}^{(0)}\rangle\langle\Psi_{k'}^{(0)}|, \tag{2.29}$$

which may be interpreted as an infinite-dimensional matrix acting in the $\mathcal{F}_s(\mathcal{H})$ Hilbert space. Then, label by $\hat{H}_0$ the diagonal elements of this matrix

$$\hat{H}_0 = \sum_{k}^{\infty} |\Psi_k^{(0)}\rangle\langle\Psi_k^{(0)}|\hat{H}|\Psi_k^{(0)}\rangle\langle\Psi_k^{(0)}|, \tag{2.30}$$

and importantly $\hat{H}_0|\Psi_k^{(0)}\rangle = \langle\Psi_k^{(0)}|\hat{H}|\Psi_k^{(0)}\rangle|\Psi_k^{(0)}\rangle, \quad \forall|\Psi_k^{(0)}\rangle \in \mathcal{F}_s(\mathcal{H})$. In other words, all $|\Psi_k^{(0)}\rangle \in \mathcal{F}_s(\mathcal{H})$ are eigenstates of $\hat{H}_0$ with eigenvalues $\langle\Psi_k^{(0)}|\hat{H}|\Psi_k^{(0)}\rangle$, which are computable, therefore choosing $\hat{H}_0$ as the unperturbed Hamiltonian is sensible. Continuing on this track, the perturbation may be identified as

$$\begin{aligned}
\hat{V} = \hat{H} - \hat{H}_0 &= \sum_{k',k''} |\Psi_{k'}^{(0)}\rangle\langle\Psi_{k'}^{(0)}| \left(\hat{H} - \sum_k |\Psi_k^{(0)}\rangle\langle\Psi_k^{(0)}|\hat{H}|\Psi_k^{(0)}\rangle\langle\Psi_k^{(0)}| \right) |\Psi_{k''}^{(0)}\rangle\langle\Psi_{k''}^{(0)}| \\
&= \sum_{k',k''} |\Psi_{k'}^{(0)}\rangle\langle\Psi_{k'}^{(0)}|\hat{H}|\Psi_{k''}^{(0)}\rangle\langle\Psi_{k''}^{(0)}| \\
&\quad - \sum_{k,k',k''} |\Psi_{k'}^{(0)}\rangle\langle\Psi_{k'}^{(0)}|\Psi_k^{(0)}\rangle\langle\Psi_k^{(0)}|\hat{H}|\Psi_k^{(0)}\rangle\langle\Psi_k^{(0)}|\Psi_{k''}^{(0)}\rangle\langle\Psi_{k''}^{(0)}| \\
&= \sum_{k',k''} |\Psi_{k'}^{(0)}\rangle\langle\Psi_{k'}^{(0)}|\hat{H}|\Psi_{k''}^{(0)}\rangle\langle\Psi_{k''}^{(0)}| - \sum_k |\Psi_k^{(0)}\rangle\langle\Psi_k^{(0)}|\hat{H}|\Psi_k^{(0)}\rangle\langle\Psi_k^{(0)}| \\
&= \sum_{\substack{k,k' \\ k\neq k'}} |\Psi_{k'}^{(0)}\rangle\langle\Psi_{k'}^{(0)}|\hat{H}|\Psi_k^{(0)}\rangle\langle\Psi_k^{(0)}|,
\end{aligned} \tag{2.31}$$

corresponding to the off-diagonal elements of the matrix $\hat{H}$. With this perturbation in hand the theory proceeds along the same line as RSPT above, however with a different perturbation and the restrictions that only matrix elements between differing states $\langle\Psi_k^{(0)}|\hat{V}|\Psi_{k'}^{(0)}\rangle$ are allowed.

Chapter 3

Applying many-body perturbation theory to the Gross-Pitaevskii equation

We start by self-consistently solving the two-component GP equation (2.16) in a basis $\{|\chi_n\rangle\}, n = 0, 1, \ldots, M-1$ of size M to obtain the eigenstates $\{|\phi_{A_n}\rangle\} \in \mathcal{F}_s^{(A)}(\mathcal{H})$, $\{|\phi_{B_n}\rangle\} \in \mathcal{F}_s^{(B)}(\mathcal{H})$ and eigenvalues $\{\mu_{A_n}\}$, $\{\mu_{B_n}\}$ of each component. Here $|\phi_{A_0}\rangle$ and $|\phi_{B_0}\rangle$ are the ground states of each components, and the goal is now to use the remaining $M-1$ eigenstates of each component to perturbatively go beyond the mean-field description. Note, that in principle one could use different bases for $\{|\phi_{A_n}\rangle\}$ and $\{|\phi_{B_n}\rangle\}$ with different basis sizes, however this will not be necessary for the systems we consider later on.

Only the two-component case is covered in this chapter as it also encompasses the one-component case. Further extension to additional components is straight forward.

3.1 Rayleigh-Schrödinger perturbation theory

Starting with the Rayleigh-Schrödinger approach where the many-body mean-field Hamiltonian is taken as the unperturbed system. This unperturbed Hamiltonian is constructed as in Eq. (2.11) by summing over the one-body Hamiltonians in the GP equation (2.16) resulting in

$$\begin{aligned}\hat{H}_{\mathrm{MF}} = &\sum_{i=1}^{N_A}\left(\hat{h} + g_{AA}(N_A-1)|\phi_{A_0}(x_i^{(A)})|^2 + g_{AB}N_B|\phi_{B_0}(x_i^{(A)})|^2\right) \\ &+ \sum_{i=1}^{N_B}\left(\hat{h} + g_{BB}(N_B-1)|\phi_{B_0}(x_i^{(B)})|^2 + g_{AB}N_A|\phi_{A_0}(x_i^{(B)})|^2\right).\end{aligned} \tag{3.1}$$

Note that this approach to perturbation theory is equivalent to the well known Møller-Plesset perturbation theory, except for bosons instead of fermions [32]. The unperturbed many-body states may then be taken as

$$|\Psi_n^{(0)}\rangle = |n_{A_0}, n_{A_1}, \ldots\rangle \otimes |n_{B_0}, n_{B_1}, \ldots\rangle \in \mathcal{F}_s^{(AB)}(\mathcal{H}), \tag{3.2}$$

with eigenvalues

$$\hat{H}_{\mathrm{MF}}|\Psi_n^{(0)}\rangle = \sum_{i=1}^{M} \left(\mu_{A_i} n_{A_i} + \mu_{B_i} n_{B_i}\right) |\Psi_n^{(0)}\rangle. \tag{3.3}$$

Using the full many-body Hamiltonian $\hat{H}$ given by Eq. (2.6), the perturbation $\hat{V}_{\mathrm{RS}}$ satisfying $\hat{H} = \hat{H}_{\mathrm{MF}} + \hat{V}_{\mathrm{RS}}$ can be identified as

$$\begin{aligned}
\hat{V}_{\mathrm{RS}} = &\sum_{i<j}^{N_A} g_{AA}\delta(x_i^{(A)} - x_j^{(A)}) - \sum_{i}^{N_A} g_{AA}(N_A - 1)|\phi_{A_0}(x_i^{(A)})|^2 \\
&+ \sum_{i<j}^{N_B} g_{BB}\delta(x_i^{(B)} - x_j^{(B)}) - \sum_{i}^{N_B} g_{BB}(N_B - 1)|\phi_{B_0}(x_i^{(B)})|^2 \\
&+ \sum_{i}^{N_A}\sum_{j}^{N_B} g_{AB}\delta(x_i^{(A)} - x_j^{(B)}) - \sum_{i}^{N_A} g_{AB}N_B|\phi_{B_0}(x_i^{(A)})|^2 \\
&- \sum_{i}^{N_B} g_{AB}N_A|\phi_{A_0}(x_j^{(B)})|^2.
\end{aligned} \tag{3.4}$$

Next, Eq. (3.4) may be expressed in second quantization as

$$\begin{aligned}
\hat{V}_{\mathrm{RS}} = &\frac{1}{2} g_{AA} \sum_{ijkl} v_{ijkl}^{(AA)} \hat{a}_{A_i}^\dagger \hat{a}_{A_j}^\dagger \hat{a}_{A_l} \hat{a}_{A_k} - g_{AA}(N_A - 1) \sum_{ij} v_{i0j0}^{(AA)} \hat{a}_{A_i}^\dagger \hat{a}_{A_j} \\
&+ \frac{1}{2} g_{BB} \sum_{ijkl} v_{ijkl}^{(BB)} \hat{a}_{B_i}^\dagger \hat{a}_{B_j}^\dagger \hat{a}_{B_l} \hat{a}_{B_k} - g_{BB}(N_B - 1) \sum_{ij} v_{i0j0}^{(BB)} \hat{a}_{B_i}^\dagger \hat{a}_{B_j} \\
&+ g_{AB} \sum_{ijkl} v_{ijkl}^{(AB)} \hat{a}_{A_i}^\dagger \hat{a}_{B_j}^\dagger \hat{a}_{B_l} \hat{a}_{A_k} - g_{AB} N_B \sum_{ij} v_{i0j0}^{(AB)} \hat{a}_{A_i}^\dagger \hat{a}_{A_j} \\
&- g_{AB} N_A \sum_{ij} v_{i0j0}^{(BA)} \hat{a}_{B_i}^\dagger \hat{a}_{B_j}
\end{aligned} \tag{3.5}$$

where the integral $v_{ijkl}^{(PQ)}$ is given by Eq. (2.9). Note that the integral $v_{ijkl}^{(PQ)}$ has some useful symmetry properties in the intra-component case where $P = Q$. Namely $v_{ijkl}^{(PP)} = v_{jikl}^{(PP)} = v_{jilk}^{(PP)} = v_{ijlk}^{(PP)}$ which as it happens, is the same symmetry as the creation and annihilation operators $\hat{a}_{P_i}^\dagger \hat{a}_{Q_j}^\dagger \hat{a}_{Q_l} \hat{a}_{P_k}$. This allows for the reduction of terms in the sums $\sum_{ijkl}(\ldots)$ and $\sum_{ij}(\ldots)$ above, greatly aiding future computational efforts.

If we now consider the matrix elements $\langle\Psi_k^{(0)}|\hat{V}|\Psi_{k'}^{(0)}\rangle$ for $|\Psi_k^{(0)}\rangle, |\Psi_{k'}^{(0)}\rangle \in \mathcal{F}_s^{(AB)}(\mathcal{H})$, needed for calculating the perturbative energy shifts ΔE, a few things can be noted. Firstly, we arrive at expressions of the form

$$\begin{aligned}
&\sum_{ijkl} \langle\Psi_k^{(0)}|\hat{a}_{A_i}^\dagger \hat{a}_{A_j}^\dagger \hat{a}_{A_l} \hat{a}_{A_k}|\Psi_{k'}^{(0)}\rangle, \quad \sum_{ij} \langle\Psi_k^{(0)}|\hat{a}_{A_i}^\dagger \hat{a}_{A_j}|\Psi_{k'}^{(0)}\rangle, \\
&\sum_{ijkl} \langle\Psi_k^{(0)}|\hat{a}_{A_i}^\dagger \hat{a}_{B_j}^\dagger \hat{a}_{B_l} \hat{a}_{A_k}|\Psi_{k'}^{(0)}\rangle,
\end{aligned} \tag{3.6}$$

and similarly for the B component. These sums are only non-zero when $|\Psi_k^{(0)}\rangle$ and $|\Psi_{k'}^{(0)}\rangle$ differ in at most two occupations. Secondly, if we take $|\Psi_0^{(0)}\rangle = |N_A, 0, \ldots\rangle \otimes |N_B, 0, \ldots\rangle$ as our unperturbed many-body ground state, then $\langle\Psi_k^{(0)}|\hat{V}|\Psi_0^{(0)}\rangle$ is only non-zero when $|\Psi_k^{(0)}\rangle$ is a double substitution. Single substitutions will be shown to be zero shortly.

We may now begin computing the perturbative energy shifts with respect to the unperturbed many-body ground state $|\Psi_0^{(0)}\rangle$ we just introduced. The unperturbed energy is simply given by the eigenvalue of $|\Psi_0^{(0)}\rangle$, see Eq. (3.3), as

$$E_0^{(0)} = \langle\Psi_0^{(0)}|\hat{H}_{\mathrm{MF}}|\Psi_0^{(0)}\rangle = N_A\mu_{A_0} + N_B\mu_{B_0}. \tag{3.7}$$

Likewise, using Eq. (2.26) the first order energy shift is quickly obtained as

$$\begin{aligned}\Delta E_0^{(1)} = \langle\Psi_0^{(0)}|\hat{V}|\Psi_0^{(0)}\rangle = &-\frac{1}{2}g_{AA}N_A(N_A-1)v_{0000}^{(AA)} - \frac{1}{2}g_{BB}N_B(N_B-1)v_{0000}^{(BB)} \\ &- g_{AB}N_AN_Bv_{0000}^{(AB)}.\end{aligned} \tag{3.8}$$

Next, in computing the second order energy shift $\Delta E_0^{(2)}$, terms of the form $\langle\Psi_k^{(0)}|\hat{V}|\Psi_0^{(0)}\rangle$ appear, and as previously mentioned $|\Psi_k^{(0)}\rangle$ must then be a double substitution. As single substitutions are expected to be zero, analogous to Brillouin's Theorem for fermions [11]. To confirm this, we label single substitutions in the A component by,

$$|A_m\rangle = \frac{1}{\sqrt{N_A}}\hat{a}_{A_m}^\dagger\hat{a}_{A_0}|\Psi_0^{(0)}\rangle \tag{3.9}$$

by moving a particle from $|\phi_{A_0}\rangle$ to $|\phi_{A_m}\rangle$. The only possible single substitution that can appear in component A is

$$\langle A_m|\hat{V}|\Psi_0^{(0)}\rangle = g_{AA}\sqrt{N_A}(N_A-1)v_{m000}^{(AA)} - g_{AA}\sqrt{N_A}(N_A-1)v_{m000}^{(AA)} = 0, \tag{3.10}$$

and likewise for the B component, confirming that the matrix elements between single substitutions and the ground state are zero for bosons as well. In a similar manner as previously, double substitutions may be labeled by

$$|A_mA_n\rangle = \frac{1}{\sqrt{N_A(N_A-1)}}\hat{a}_{A_m}^\dagger\hat{a}_{A_n}^\dagger\hat{a}_{A_0}\hat{a}_{A_0}|\Psi_0^{(0)}\rangle, \tag{3.11}$$

$$|A_mA_m\rangle = \frac{1}{\sqrt{2}}\frac{1}{\sqrt{N_A(N_A-1)}}\hat{a}_{A_m}^\dagger\hat{a}_{A_m}^\dagger\hat{a}_{A_0}\hat{a}_{A_0}|\Psi_0^{(0)}\rangle, \tag{3.12}$$

$$|A_mB_n\rangle = \frac{1}{\sqrt{N_AN_B}}\hat{a}_{A_m}^\dagger\hat{a}_{B_n}^\dagger\hat{a}_{B_0}\hat{a}_{A_0}|\Psi_0^{(0)}\rangle, \tag{3.13}$$

for the cases where two bosons reside in different one-body states $|\phi_{A_m}\rangle, |\phi_{A_n}\rangle$, the same state $|\phi_{A_m}\rangle, |\phi_{A_m}\rangle$, and lastly different components $|\phi_{A_m}\rangle, |\phi_{B_n}\rangle$. The matrix elements

$\langle \Psi_k^{(0)} | \hat{V} | \Psi_0^{(0)} \rangle$ where $|\Psi_k^{(0)}\rangle$ is a double substitution may then be calculated resulting in

$$\langle A_m A_m | \hat{V} | \Psi_0^{(0)} \rangle = \frac{1}{\sqrt{2}} g_{AA} \sqrt{N_A(N_A-1)} v_{mm00}^{(AA)}, \tag{3.14}$$

$$\langle A_m A_n | \hat{V} | \Psi_0^{(0)} \rangle = g_{AA} \sqrt{N_A(N_A-1)} v_{mn00}^{(AA)}, \tag{3.15}$$

$$\langle A_m B_n | \hat{V} | \Psi_0^{(0)} \rangle = g_{AB} \sqrt{N_A N_B} v_{mn00}^{(AB)}, \tag{3.16}$$

where matrix elements with respect to only the B component take the same form as Eq. (3.16) and (3.15) due to their symmetry with the A. Applying the above notation, the second order energy shift $\Delta E_0^{(2)}$ with respect to the unperturbed many-body ground state $|\Psi_0^{(0)}\rangle$, given by Eq. (2.27), can be written as

$$\begin{aligned} \Delta E_0^{(2)} = &\sum_{m \leq n} \frac{|\langle A_m A_n | \hat{V} | \Psi_0^{(0)} \rangle|^2}{2\mu_{A_0} - \mu_{A_m} - \mu_{A_n}} + \sum_{m \leq n} \frac{|\langle B_m B_n | \hat{V} | \Psi_0^{(0)} \rangle|^2}{2\mu_{B_0} - \mu_{B_m} - \mu_{B_n}} \\ &+ \sum_{m,n} \frac{|\langle A_m B_n | \hat{V} | \Psi_0^{(0)} \rangle|^2}{\mu_{A_0} + \mu_{B_0} - \mu_{A_m} - \mu_{B_n}}, \end{aligned} \tag{3.17}$$

where the sums run over all permissible indices in the range $[1, M-1]$.

Lastly, from Eq. (2.28) we see that the matrix elements required for the third order energy shift $\Delta E_0^{(3)}$ take the form $\langle \Psi_0^{(0)} | \hat{V} | \Psi_k^{(0)} \rangle \langle \Psi_k^{(0)} | \hat{V} | \Psi_{k'}^{(0)} \rangle \langle \Psi_{k'}^{(0)} | \hat{V} | \Psi_0^{(0)} \rangle$,$\langle \Psi_0^{(0)} | \hat{V} | \Psi_0^{(0)} \rangle$, and $\langle \Psi_k^{(0)} | \hat{V} | \Psi_0^{(0)} \rangle$. The latter two matrix elements have already been evaluated. For the former, we know that $\langle \Psi_k^{(0)} | \hat{V} | \Psi_0^{(0)} \rangle = 0$ for single substitutions and as such only the case where $|\Psi_k^{(0)}\rangle$ and $|\Psi_{k'}^{(0)}\rangle$ are double substitutions needs to be considered. This is done in detail in Appendix B since there are a lot of permutations to consider, and the computations become quite lengthy.

In terms of actually computing the third order energy shift, Eq. (2.28) is suboptimal as it requires us to evaluate the costly matrix elements for each term in the sum. This is especially problematic as a lot of our matrix elements will be equal due to the symmetry of $v_{ijkl}^{(PQ)}$. We therefore restructure Eq. (2.28) into a form more suitable for high performance computing which makes more efficient use of the matrix elements. In the one-component case the energy shift for component A takes to form

$$\begin{aligned} \Delta E_0^{(3),(AA)} = &g_{AA} v_{0000}^{(AA)} \sum_{m \leq n} [t_{mn}^{(AA)}]^2 \\ &+ g_{AA}(N_A - 3) \sum_{m,n} v_{m0n0}^{(AA)} \sum_p t_{mp}^{(AA)} t_{np}^{(AA)} \\ &\quad \times \left\{ 1 + (\sqrt{2}-1)(\delta_{m,p} + \delta_{n,p}) + (3 - 2\sqrt{2}) \delta_{m,p} \delta_{n,p} \right\} \\ &+ g_{AA} \sum_{\substack{m \leq n \\ p \leq q}} v_{mnpq}^{(AA)} t_{mn}^{(AA)} t_{pq}^{(AA)} \\ &\quad \times \left\{ 2 + (\sqrt{2}-2)(\delta_{m,n} + \delta_{p,q}) + (3 - 2\sqrt{2}) \delta_{m,n} \delta_{p,q} \right\}, \end{aligned} \tag{3.18}$$

with sums running over integrals $v_{ijkl}^{(PQ)}$ instead of permutations of states as in Eq. (2.28).

In the above

$$t_{ij}^{(PQ)} = \frac{\langle P_i Q_j | \hat{V} | \Psi_0^{(0)} \rangle}{\mu_{P_0} + \mu_{Q_0} - \mu_{P_i} - \mu_{Q_j}} \tag{3.19}$$

was introduced to simplify calculations. Additionally, the matrix element $\langle P_i Q_j | \hat{V} | \Psi_0^{(0)} \rangle$ in $t_{ij}^{(PQ)}$ may be reused from the calculations of the second order energy shift, greatly reducing computation time. Similarly, in the two-component case, contributions from inter-component terms may be added resulting in

$$\begin{aligned}
\Delta E_0^{(3)} = \Delta E_0^{(3),(AA)} &+ \Delta E_0^{(3),(BB)} \\
&+ g_{AB} v_{0000}^{(AB)} \sum_{m,n} [t_{mn}^{(AB)}]^2 \\
&+ \sum_{m,n} \left(g_{AA}(N_A - 1) v_{m0n0}^{(AA)} - g_{AB} v_{m0n0}^{(AB)} \right) \sum_p t_{mp}^{(AB)} t_{np}^{(AB)} \\
&+ \sum_{m,n} \left(g_{BB}(N_B - 1) v_{m0n0}^{(BB)} - g_{AB} v_{0m0n}^{(AB)} \right) \sum_p t_{pm}^{(AB)} t_{pn}^{(AB)} \\
&+ g_{AB} \sum_{m,n,p,q} v_{mnpq}^{(AB)} t_{mn}^{(AB)} t_{pq}^{(AB)}
\end{aligned} \tag{3.20}$$

for two-components.

3.2 Epstein-Nesbet perturbation theory

If we instead use the Epstein-Nesbet partitioning as covered in Sec. 2.4.2 and start from the same full many-body Hamiltonian $\hat{H}$ given by Eq. (2.7) in second quantization, the perturbation $\hat{V}_{\mathrm{EN}}$ is given by (2.31). Now adding $0 = \hat{H}_{\mathrm{MF}} - \hat{H}_{\mathrm{MF}}$ to $\hat{H}$, where $\hat{H}_{\mathrm{MF}}$ is the many-body mean-field Hamiltonian Eq. (3.1), one gets

$$\begin{aligned}
\hat{V}_{\mathrm{EN}} &= \sum_{\substack{k,k' \\ k \neq k'}} |\Psi_{k'}^{(0)}\rangle \langle \Psi_{k'}^{(0)} | \hat{H} | \Psi_k^{(0)} \rangle \langle \Psi_k^{(0)}| \\
&= \sum_{\substack{k,k' \\ k \neq k'}} |\Psi_{k'}^{(0)}\rangle \langle \Psi_{k'}^{(0)} | \hat{H} + \hat{H}_{\mathrm{MF}} - \hat{H}_{\mathrm{MF}} | \Psi_k^{(0)} \rangle \langle \Psi_k^{(0)}| \\
&= \sum_{\substack{k,k' \\ k \neq k'}} |\Psi_{k'}^{(0)}\rangle \langle \Psi_{k'}^{(0)} | \hat{V}_{\mathrm{RS}} + \hat{H}_{\mathrm{MF}} | \Psi_k^{(0)} \rangle \langle \Psi_k^{(0)}| \\
&= \sum_{\substack{k,k' \\ k \neq k'}} |\Psi_{k'}^{(0)}\rangle \langle \Psi_{k'}^{(0)} | \hat{V}_{\mathrm{RS}} | \Psi_k^{(0)} \rangle \langle \Psi_k^{(0)}|,
\end{aligned} \tag{3.21}$$

where $\hat{V}_{\mathrm{RS}} = \hat{H} - \hat{H}_{\mathrm{MF}}$ is the Rayleigh-Schrödinger perturbation given by Eq. (3.5). In the last equality the fact that $|\Psi_k^{(0)}\rangle$ is an eigenstate of $\hat{H}_{\mathrm{MF}}$ was used, meaning $\langle \Psi_{k'}^{(0)} | \hat{H}_{\mathrm{MF}} | \Psi_k^{(0)} \rangle = 0$ when $k \neq k'$. All in all, this means that the matrix elements $\langle \Psi_{k'}^{(0)} | \hat{V}_{\mathrm{EN}} | \Psi_k^{(0)} \rangle$ are equal to $\langle \Psi_{k'}^{(0)} | \hat{V}_{\mathrm{RS}} | \Psi_k^{(0)} \rangle$ when $|\Psi_{k'}^{(0)}\rangle \neq |\Psi_k^{(0)}\rangle$, and all previous calcu-

lations of these matrix elements may be used, simplifying calculations considerably. We may then use Eq. (3.7), (3.8), (3.17), and (3.20) to also calculate the ENPT energy shifts, as long as we remember to change the unperturbed energies in the denominator, and exclude matrix elements between the same states.

All that now remains in ENPT, is the calculation of the new unperturbed eigenvalues $\langle\Psi_k^{(0)}|\hat{H}|\Psi_k^{(0)}\rangle$. As the perturbation is the same as in RSPT the only states $|\Psi_k^{(0)}\rangle$ that need to be considered are the unperturbed ground state $|\Psi_0^{(0)}\rangle = |N_A, 0, \ldots\rangle \otimes |N_B, 0, \ldots\rangle$, and the double substitutions $|A_m A_m\rangle$, $|A_m A_n\rangle$, $|A_m B_n\rangle$. Starting with the ground state

$$\begin{aligned}\langle\Psi_0^{(0)}|\hat{H}|\Psi_0^{(0)}\rangle = N_A h_{00}^{(A)} &+ \frac{1}{2} g_{AA} N_A (N_A - 1) v_{0000}^{(AA)} \\ &+ N_B h_{00}^{(B)} + \frac{1}{2} g_{BB} N_B (N_B - 1) v_{0000}^{(BB)} \\ &+ g_{AB} N_A N_B v_{0000}^{(AB)},\end{aligned} \tag{3.22}$$

and next the double substitutions within one component

$$\begin{aligned}\langle A_m A_n|\hat{H}|A_m A_n\rangle = h_{mm}^{(A)} + h_{nn}^{(A)} &+ (N_A - 2) h_{00}^{(A)} \\ &+ \frac{1}{2} g_{AA} \Big(4 v_{mnmn}^{(AA)} + 4(N_A - 2) v_{m0m0}^{(AA)} \\ &\qquad + 4(N_A - 2) v_{n0n0}^{(AA)} + (N_A - 2)(N_A - 3) v_{0000}^{(AA)} \Big) \\ &+ N_B h_{00}^{(B)} + \frac{1}{2} g_{BB} N_B (N_B - 1) v_{0000}^{(BB)} \\ &+ g_{AB} N_B \left(v_{m0m0}^{(AB)} + v_{n0n0}^{(AB)} + (N_A - 2) v_{0000}^{(AB)} \right).\end{aligned} \tag{3.23}$$

Likewise, if $m = n$ we get

$$\begin{aligned}\langle A_m A_m|\hat{H}|A_m A_m\rangle = 2h_{mm}^{(A)} &+ (N_A - 2) h_{00}^{(A)} \\ &+ \frac{1}{2} g_{AA} \Big(2 v_{mmmm}^{(AA)} + 8(N_A - 2) v_{m0m0}^{(AA)} \\ &\qquad + (N_A - 2)(N_A - 3) v_{0000}^{(AA)} \Big) \\ &+ N_B h_{00}^{(B)} + \frac{1}{2} g_{BB} N_B (N_B - 1) v_{0000}^{(BB)} \\ &+ g_{AB} N_B \left(2 v_{m0m0}^{(AB)} + (N_A - 2) v_{0000}^{(AB)} \right).\end{aligned} \tag{3.24}$$

Note that setting $N_B = 0$ yields the one-component case. Moving on, if a single substitu-

tion occurs in each component, the energy becomes

$$\begin{aligned}\langle A_m B_n|\hat{H}|A_m B_n\rangle &= h^{(A)}_{mm} + (N_A-1)h^{(A)}_{00} \\ &\quad + \frac{1}{2}g_{AA}\left(4(N_A-1)v^{(AA)}_{m0m0} + (N_A-1)(N_A-2)v^{(AA)}_{0000}\right) \\ &\quad + h^{(B)}_{nn} + (N_B-1)h^{(B)}_{00} \\ &\quad + \frac{1}{2}g_{BB}\left(4(N_B-1)v^{(BB)}_{n0n0} + (N_B-1)(N_B-2)v^{(BB)}_{0000}\right) \\ &\quad + g_{AB}\Big((N_B-1)v^{(AB)}_{m0m0} + (N_A-1)v^{(AB)}_{0n0n} + v^{(AB)}_{mnmn} \\ &\qquad\qquad +(N_A-1)(N_B-1)v^{(AB)}_{0000}\Big)\,.\end{aligned} \tag{3.25}$$

With the above energies calculated, the energy difference appearing in the denominator of the perturbative energy shifts is given by

$$\begin{aligned}\langle\Psi^{(0)}_0|\hat{H}|\Psi^{(0)}_0\rangle - \langle A_m A_n|\hat{H}|A_m A_n\rangle &= 2h^{(A)}_{00} - h^{(A)}_{mm} - h^{(A)}_{nn} \\ &\quad - g_{AA}\Big((2-\delta_{m,n})v^{(AA)}_{mnmn} + 2(N_A-2)(v^{(AA)}_{m0m0} + v^{(AA)}_{n0n0}) \\ &\qquad\qquad -(2N_A-3)v^{(AA)}_{0000}\Big) \\ &\quad - g_{AB}N_B\left(v^{(AB)}_{m0m0} + v^{(AB)}_{n0n0} - 2v^{(AB)}_{0000}\right)\end{aligned} \tag{3.26}$$

in the case where both excitations occur within one component, and

$$\begin{aligned}\langle\Psi^{(0)}_0|\hat{H}|\Psi^{(0)}_0\rangle - \langle A_m B_n|\hat{H}|A_m B_n\rangle &= h^{(A)}_{00} - h^{(A)}_{mm} - g_{AA}\left(2(N_A-1)v^{(AA)}_{m0m0} - (N_A-1)v^{(AA)}_{0000}\right) \\ &\quad + h^{(B)}_{00} - h^{(B)}_{nn} - g_{BB}\left(2(N_B-1)v^{(BB)}_{n0n0} - (N_B-1)v^{(BB)}_{0000}\right) \\ &\quad - g_{AB}\Big(v^{(AB)}_{mnmn} + (N_B-1)v^{(AB)}_{m0m0} + (N_A-1)v^{(AB)}_{0n0n} \\ &\qquad\qquad -(N_A+N_B-1)v^{(AB)}_{0000}\Big)\end{aligned} \tag{3.27}$$

if an excitation occurs within each component.

Lastly, we motivate the reason to study ENPT in the first place. For RSPT we obtain the GP energy if we include corrections up to first order

$$\begin{aligned}E_0^{(\mathrm{RSPT0})} + \Delta E_0^{(\mathrm{RSPT1})} &= \langle\Psi^{(0)}_0|\hat{H}_{\mathrm{MF}}|\Psi^{(0)}_0\rangle + \langle\Psi^{(0)}_0|\hat{V}_{\mathrm{RS}}|\Psi^{(0)}_0\rangle \\ &= \langle\Psi^{(0)}_0|\hat{H}_{\mathrm{MF}} + \hat{V}_{\mathrm{RS}}|\Psi^{(0)}_0\rangle \\ &= E_{\mathrm{GP}}\end{aligned}\,, \tag{3.28}$$

whereas for ENPT we get

$$\begin{aligned} E_0^{(\mathrm{ENPT0})} &= \langle \Psi_0^{(0)} | \hat{H} - \hat{V}_{\mathrm{EN}} | \Psi_0^{(0)} \rangle = \langle \Psi_0^{(0)} | \hat{H} | \Psi_0^{(0)} \rangle - \langle \Psi_0^{(0)} | \hat{V}_{\mathrm{EN}} | \Psi_0^{(0)} \rangle \\ &= \langle \Psi_0^{(0)} | \hat{H} | \Psi_0^{(0)} \rangle \\ &= E_{\mathrm{GP}} \end{aligned} \tag{3.29}$$

by only including zeroth order terms. We therefore expect ENPT to scale better with perturbative order, and as the unperturbed eigenvalues are more accurate we moreover expect a more accurate weighting of the terms in the ENPT perturbative series.

Chapter 4

Evaluation of beyond mean-field methods

This chapter starts out by discussing particular details relevant to the implementation of the SCF and MBPT methods in Sec. 4.1, before moving on to verify the accuracy of the SCF method in Sec. 4.2. Similarly, in Secs. 4.3 and 4.4 the MBPT methods are verified against the FCI method and mean-field energies in the low- and high particle-number regimes respectively. Sec. 4.5 concludes the examination of the MBPT methods by looking at their scaling behavior with respect to increasing interaction strengths for a fixed particle count. Finally, a case study of more complicated systems is conducted in Sec. 4.6.

4.1 Implementation details

All computations in this thesis, be that SCF or MBPT, are performed in the basis of Harmonic Oscillator (HO) eigenfunctions, motivated by the experimental relevance of working in a harmonic potential $u(x) = \frac{1}{2}\omega x^2$. The n:th HO basis function $\chi_n(x)$ is analytically known as

$$\chi_n(x) = \frac{1}{\sqrt{2^n n!}} \left(\frac{\omega}{\pi}\right)^{1/4} \exp(-\omega x^2/2) H_n(\sqrt{\omega}x), \tag{4.1}$$

where the Hermite polynomials $H_n(x)$ are most easily computed via the iterative scheme

$$H_{n+1}(x) = 2xH_n(x) - 2nH_{n-1}(x), \tag{4.2}$$

with $H_0(x) = 1, H_1(x) = 2x$ as a starting point. Numerically speaking, this iterative approach is favored over the explicit form of $H_n(x)$ with its many factorials, which are time-consuming to compute.

Both the SCF and MBPT methods necessitate the computation of matrix elements between states of the form

$$\langle \phi_m | \hat{o} | \phi_n \rangle = \int \mathrm{d}x \, \phi_m^*(x) \hat{o}(x) \phi_n(x), \tag{4.3}$$

for some operator $\hat{o}$. Most integrals were computed numerically using an adaptive Gauss-Kronod quadrature of order 20 [48], with the exception of the integrals $v_{ijkl}^{(MN)}$ given by

Eq. (2.9) which were most efficiently computed in the HO basis using the analytical expression derived in Appendix D. The drawback in the latter case is a loss of generality with respect to the choice of basis functions. Another important numerical aspect of this implementation, is the efficient solving of eigenvalue problems which were carried out by either the ARPACK package or OPENBLAS which implement the LAPACK and BLAS APIs [49, 50, 51]. Parallelization was performed using either OPENMP or in more critical regions CUDA [52, 53].

All code is open source and available at `https://github.com/AntonJohansson/sbmf`. However as most of the interesting functions implementing the MBPT methods are heavily optimized and quite terse, Appendix C contains a pseudo code implementation of the third order RSPT computations, and briefly discusses some optimization opportunities.

4.1.1 Determining convergence

Lastly, some details regarding convergence: The implemented SCF method relies on an absolute error criterion whilst the numerical integration method uses both an absolute and relative error criterion. These criteria are specified in the following way: If x_i is the value produced by the i:th iteration (x_i could also be vector valued as for SCF) then the absolute error criteria is $||x_{i+1} - x_i|| < \epsilon_{\text{abs}}$ and the relative criterion by $||x_{i+1} - x_i||/||x_i|| < \epsilon_{\text{rel}}$, where $\epsilon_{\text{abs}}, \epsilon_{\text{rel}}$ are the desired error tolerances. Including both criterion allows for faster convergence since the relative error is more efficient for larger x_i but struggles when x_i is close to 0, which is why the absolute error is included. For this reason $\epsilon_{\text{abs}} < \epsilon_{\text{rel}}$ was chosen such that the absolute error is used for small whilst the relative error is used for larger values. Convergence of the SCF method was then determined by the absolute criterion $||\mathbf{c}^{(i+1)} - \mathbf{c}^{(i)}|| < 10^{-14}$, where the vector $\mathbf{c}^{(i)}$ denotes the expansion coefficients of the estimated eigenstate $|\phi^{(i)}\rangle = \sum_n c_n^{(i)} |\chi_n\rangle$ at the i:th iteration. A relative error criterion is however not applicable as the states are normalized meaning $||\mathbf{c}^{(i)}|| = 1$. Lastly, for numerical integration both an absolute $\epsilon_{\text{abs}} = 10^{-15}$ and relative $\epsilon_{\text{rel}} = 10^{-8}$ criterion was used, calculated from the estimated integral at each iteration.

4.2 Convergence and correctness of the implemented self-consistent field method

An important aspect of the SCF method is the choice of an initial guess to the system eigenstate $|\phi^{(0)}\rangle = \sum_{i=0}^{M-1} c_i^{(0)} |\chi_i\rangle$, that is the choice of the initial coefficient vector $\mathbf{c}^{(0)}$. All SCF computations in this thesis were performed for two different initial guesses. Firstly, choosing $|\phi^{(0)}\rangle = |\chi_0\rangle$ as the lowest eigenvalue basis state, and secondly, picking $\mathbf{c}^{(0)}$ as the lowest eigenvalue eigenvector of a random real-symmetric matrix of size $M \times M$. In the two-component case, two initial guesses were required, one for each component, and here either the two lowest eigenvalue basis states $|\chi_0\rangle, |\chi_1\rangle$ were chosen or two random initial states in the manner described previously. All systems studied in this thesis consider both options of initial guesses, and if not explicitly stated as such, both methods can be assumed to have produced the same final eigenstate.

A natural starting point in verifying the numerical implementation of our SCF method outlined in Sec. 2.3, is the investigation of a relatively simple system. To this end, a one-component BEC in a harmonic trap $u(x) = \frac{1}{2}x^2$ modeled by the GP equation (2.14) is studied. We consider $N = 4$ particles with an interaction strength of $g = 1/3$. In

solving the above system self-consistently, convergence is rapidly achieved with respect to basis size for the various initial guesses outlined above. If 16 HO basis functions are used, the ground state chemical potential is found to be $\mu = 0.86994386$ (a. u.) whilst the choice of 64 basis functions yields $\mu = 0.86994384$ (a. u.), agreement up to 7 decimal places. Moreover, overall agreement is good for all tested systems in comparison to results obtained from colleagues using a different software based on a B-spline basis, and to computations made in the GPELab MATLAB toolbox [54].

We note, however, that the convergence behavior for systems with larger coupling constants $\lambda = g(N-1)$, may become an issue. For instance, consider the above system but with an interaction strength $g = 4/3$ ($\lambda = 4$), still using 16 basis functions. Figure 4.1 shows the computed eigenvalue at each SCF iteration for this system, for multiple values of the Hamiltonian mixing parameter α and orbital mixing parameter β. See Eq. (2.22) and (2.23) for the definitions of Hamiltonian and orbital mixing. The left panel of Fig. 4.1 shows the pure SCF method without any mixing $\alpha = \beta = 0$, and a clear oscillatory behavior is seen where the method jumps between two states. As such the pure SCF method fails to converge. Note that only the first 35 iterations are shown but computations were done up to iteration 1000 without giving any different results. Next, the center panel shows results of the SCF method with non-zero Hamiltonian mixing for various values of α. Finally, the right most panel presents the SCF method with non-zero orbital mixing for various values of β. Lines ending indicate convergence, and a maximum of 1000 iterations were considered.

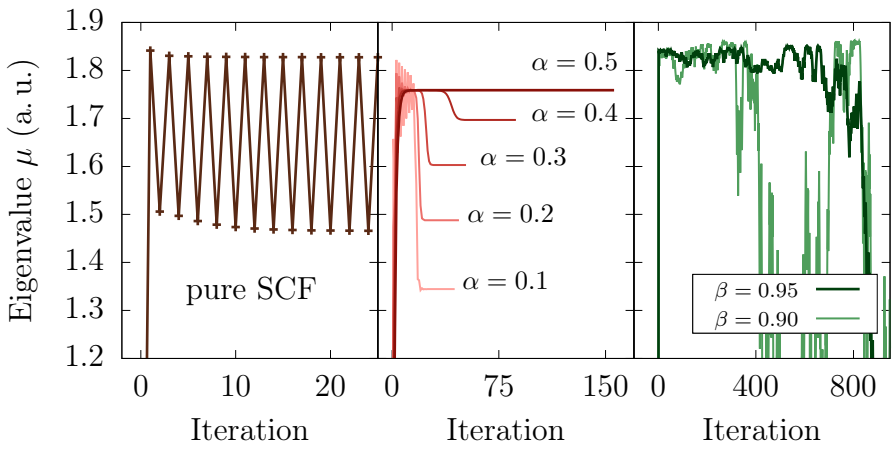

Figure 4.1: Convergence behaviour of the pure SCF method (left) with the addition of Hamiltonian mixing (center) and orbital mixing (right) for strongly interacting bosons where $\lambda = 4$. The eigenvalue μ of the ground state is shown as a function of SCF iterations. Results are also shown for multiple value of the Hamiltonian and orbital mixing parameters α and β respectively.

From the above figure, it is clear that Hamiltonian mixing improves the convergence of the SCF method, however another problem surfaces, that is Hamiltonian mixing appears to cause convergence to different chemical potentials depending on α. If α is small and we alter the Hamiltonian too much each iteration it is possible to end up with a Hamiltonian that is no longer representative of our original system. As such the state we converge towards (if we converge) is not an eigenstate of our unmixed Hamiltonian. In other

words, the resulting mixed Hamiltonian is not self-consistent with our original problem. For this system $\alpha \geq 0.5$ was sufficient to converge towards an eigenstate of our original Hamiltonian. In fact, all tested $\alpha \in [0.5, 1)$ result in the same state and chemical potential, only with different convergence rates. This corresponds to the stable region of the method and an optimal convergence rate of 40 iterations was found for $\alpha = 0.6$. On the other hand, orbital mixing appears unstable, even for very large mixing parameters β. The SCF method instead hovers above the correct μ for lower iterations but does not manage to converge and eventually becomes unstable. To answer why this is the case is difficult, as no closed form expression mapping $|\phi^{(n)}\rangle \mapsto |\phi^{(n+1)}\rangle$ exists and convergence analysis is thus no easy feat. In any case, Hamiltonian mixing is the clear favorite for dealing with unstable behaviour moving forward.

More sophisticated methods to aid in convergence such as *Direct Inversion in the Iterative Subspace* were also explored although not thoroughly enough to do the method justice, see Ref. [55] for further information.

4.3 Comparison of many-body perturbation theory to full configuration interaction

We again study the harmonically trapped one-component BEC encountered in the previous section, this time however for interaction strengths $g = \pm 1/6, \pm 1/3$ corresponding to a weakly attractive/repulsive and strongly attractive/repulsive BEC respectively. The motivation for this is twofold, firstly to see how well MBPT captures the physics of these different regimes, and secondly to investigate the convergence of the MBPT methods themselves with respect to basis size and perturbative order. To accomplish this task comparisons are made with FCI calculations which necessitates a small particle count $N = 4$.

Figure 4.2 then presents the absolute value of the relative energy difference between the ground state energy calculated from MBPT methods (E_{MBPT}) and the FCI method (E_{FCI}) as a function of basis size. The term "MBPT methods" is here used as a catchall for the implemented RSPT2, RSPT3 and ENPT2, ENPT3 methods, where the suffixed number denotes the order of the method. As an example E_{RSPT3} is calculated as $E_{\mathrm{RSPT3}} = E_0^{(\mathrm{RSPT0})} + \Delta E_0^{(\mathrm{RSPT1})} + \Delta E_0^{(\mathrm{RSPT2})} + \Delta E_0^{(\mathrm{RSPT3})}$, where the terms correspond to the unperturbed energy, and first-, second-, and third order energy shifts respectively, calculated using RSPT. Finally, four different systems are shown for interaction strengths $g = \pm 1/6, \pm 1/3$ corresponding to values of the non-linear parameter $\lambda = \pm 0.5, \pm 1$ where $\lambda = g(N-1)$. Systems are expressed in terms of λ as this factor scales the overall size of the interaction term in the mean-field Hamiltonian, and is therefore more relevant in the discussion of the perturbative methods. Note that as MBPT is non-variational, in contrast to FCI, it is possible to obtain energies lower than the correct ground state energy. This is particularly prevalent for repulsive interactions and is also the reason we are interested in the absolute rather than the signed energy difference.

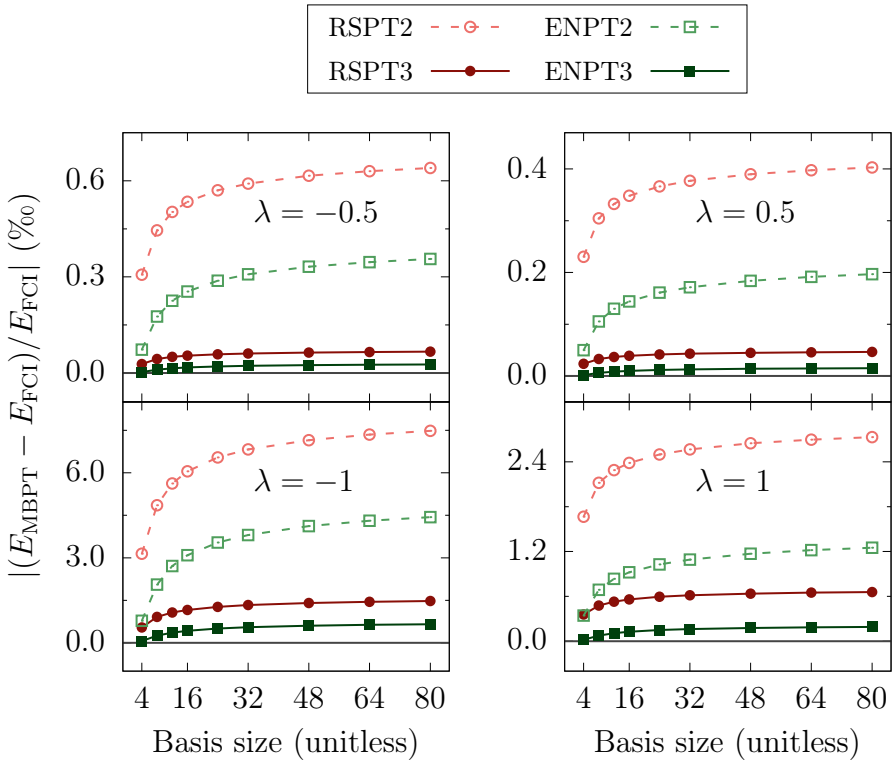

Figure 4.2: Ground state energies of a one-dimensional one-component BEC in a harmonic trap computed via the RSPT and ENPT methods to order two and three, shown as a function of basis size. Four different systems are presented for different non-linear parameters $\lambda = \pm 0.5, \pm 1$ with $N = 4$ particles. Energies are shown relative to the exact FCI energy.

From the systems studied in the above figure, we are firstly interested in when the relative error between the MBPT and FCI methods becomes basis size independent. This occurs when occurs when the error "flattens out" which appears to be the case for our third order methods for $M \geq 64$ basis functions, which we will soon confirm quantitatively. Secondly, we note generally good agreement between RSPT3, ENPT3 and FCI, the relative energy difference remains less than 1.5 ‰ even in the worst case when $\lambda = -1$. It also becomes clear that the agreement between RSPT3 and ENPT3 appears to worsen with increasing non-linear parameter $|\lambda|$ and moreover appears worse for negative compared to positive λ. For $\lambda = 0.5, -0.5$, the energies of RSPT3 and ENPT3 remain within 0.05 ‰ and 0.1 ‰ of the FCI energy respectively, compared to 0.75 ‰ and 1.5 ‰ for $\lambda = 1, -1$. The accuracy is expected to worsen with increasing $|\lambda|$ as a larger λ corresponds to a larger perturbation relative to the unperturbed Hamiltonian. As to why a negative non-linear parameter seems to worsen the accuracy, $\lambda < 0$ corresponds to attractive inter-particle interactions and the resulting unperturbed system will be more tightly bound with a lower energy. Consequently, the relative size of the perturbation is larger, resulting in worsened accuracy. Furthermore, ENPT both second- and third order appears to agree better with FCI compared to RSPT, for all λ. This is in line with what we expect from ENPT with its more accurate unperturbed energies and thus better weighting of terms in the perturbative series, as discussed in Sec. 3.2.

We thirdly want to note a few peculiarities in Fig. 4.2 which is that the relative error appears to grow with increasing basis size. An intuitive explanation of this is: because the basis size and therefore also Hilbert space of solutions is so small, there simply is not enough room for the methods to differentiate themselves. In other words, MBPT and FCI may be close in energy for smaller basis sizes, but they both constitute equally bad descriptions of the actual systems.

Lastly, we return to the question of convergence, and demonstrate that a basis consisting of 64 HO basis functions is sufficient for the considered problem. Table 4.1 presents the absolute difference in relative energy for 64 and 80 basis functions for both the RSPT3 and ENPT3 methods, using data from Fig. 4.2. As an example, if the exponent "(bf $= m$)" refers to computations made using m basis functions, then for RSPT3 the quantity of interest is

$$\left| \frac{E_{\text{RSPT3}}^{(\text{bf}=80)} - E_{\text{FCI}}^{(\text{bf}=80)}}{E_{\text{FCI}}^{(\text{bf}=80)}} - \frac{E_{\text{RSPT3}}^{(\text{bf}=64)} - E_{\text{FCI}}^{(\text{bf}=64)}}{E_{\text{FCI}}^{(\text{bf}=64)}} \right|. \tag{4.4}$$

This particular quantity is considered such that results from the table are directly comparable to the results of Fig. 4.2.

Table 4.1: Absolute difference between ground state energies relative to E_{FCI} for 64 and 80 basis functions. Computations are made using either RSPT3 or ENPT3 and the quantities presented for each method are calculated via Eq. (4.4).

λ	RSPT3 (‰)	ENPT3 (‰)
-0.5	0.00111	0.000807
0.5	0.000657	0.000439
-1.0	0.0279	0.0207
1.0	0.00875	0.00557

Both RSPT3 and ENPT3 shows satisfactory convergence with respect to basis size for 64 HO basis functions. The errors between using 64 and 80 basis functions in the table above are clearly small in comparison to the energy scales in Fig. 4.2. For reference ENPT3 has a relative error of about ≈ 0.2 ‰ for $\lambda = 1$ and 80 basis functions. Moreover, convergence appears to worsen for systems where beyond mean-field effects are particularly important, meaning convergence is worse for increasing $|\lambda|$ and especially for $\lambda < 0$.

4.4 Scaling of many-body perturbation theory with particle number

After having examined the MBPT methods for $N = 4$ particles and an interaction strength of $\lambda = \pm 0.5, \pm 1$, a natural progression is varying these parameters to get an idea of how the method fairs for more complicated systems. In particular to systems consisting of more particles. We are still considering a harmonically trapped one-component BEC. Unfortunately, FCI calculations are not computationally feasible in this regime, so we have no exact result to compare against. To provide some sense of correctness, the BeMF equation (2.20) was solved self-consistently and the fractional occupation of the BeMF

ground state n_0/N was subsequently computed. If $n_0/N = 1$ then the GP ground state is accurate and our perturbative methods start from a correct unperturbed state.

When increasing the particle count N, an interesting question is whether or not the perturbative energies approach the GP energy E_{GP}, computed from Eq. (2.13), in the mean-field limit (see Sec. 2.2.1). In this limit, $\lambda = g(N-1)$ is kept constant whilst $N \to \infty$. This scaling is investigated in Fig. 4.3 where the energy of the ENPT3 method is shown relative to E_{GP}, for particle counts $N \in [4, 160]$. Note that only ENPT3 is shown for clarity, RSPT3 performs similarly. Moreover, all computations were performed using 64 HO basis functions and for all values of N, the BeMF solution yielded a fractional occupation of $n_0/N = 1$, meaning the GP ground state is accurate.

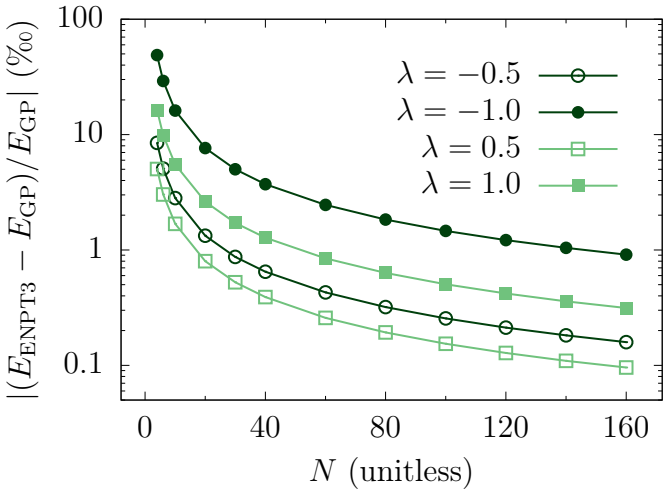

Figure 4.3: Relative energy difference of the ENPT3 method to the mean-field energy E_{GP}, for increasing particle counts N. The particle count is scaled in the mean-field limit where $\lambda = g(N-1)$ is kept constant, in this case at either $\pm 0.5, \pm 1.0$.

A clear convergence of the ENPT3 method to the mean-field energy E_{GP} is seen in Fig. 4.3, as is expected in the mean-field limit. For all values of λ, ENPT3 converged to a relative energy difference less than 1 ‰ within $N \geq 160$. Here we have run calculations up to 10000 particles and observed that the relative error continues to decrease, as expected. The speed of convergence with respect to λ is clearly related to the size of the perturbation relative to the unperturbed Hamiltonian, in exactly the same manner as discussed in Sec. 4.3.

The last part of this section will focus on the convergence of the RSPT3 and ENPT3 methods with respect to both perturbative order and basis size. Starting with perturbative order, Fig. 4.4 shows the absolute energy difference between the first- and second order, and second- and third order methods. These energy differences are again shown as a function of particle count N. The RSPT2,1 notation refers to both the RSPT2 and RSPT1 methods, and in particular the difference in energy between these methods. From Fig. 4.4 it becomes immediately clear that the energy difference between the first- and second order RSPT and ENPT methods behaves very similarly. Therefore, as ENPT exhibits a lower energy difference between the second and third order we can conclude that it has converged more with respect to perturbative order. Moreover, as the absolute error flattens out with increasing N in all cases, and the mean-field energy grows roughly linearly in N, we can conclude that the relative size of the perturbative error decreases as

we approach the mean-field limit. This is expected as we are dealing with an increasingly weakly interacting system.

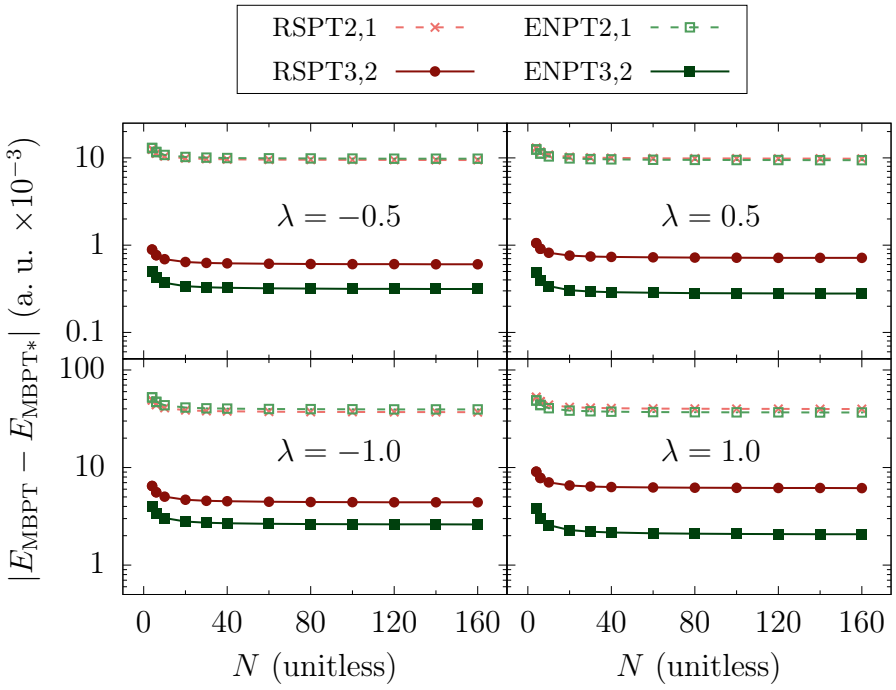

Figure 4.4: Absolute energy difference between first- and second order, and second- and third order MBPT methods. Shown as a function of particle count N. Notation-wise RSPT2,1 refers to RSPT of second and first order.

Secondly, to investigate convergence with respect to basis size, Tab. 4.2 presents the relative energy difference between 80 and 64 HO basis functions computed for RSPT3 and ENPT3. Using the same notation as previously, this table shows the quantity

$$\left| E^{(\mathrm{bf}=80)}_{\mathrm{RSPT3}} - E^{(\mathrm{bf}=64)}_{\mathrm{RSPT3}} \right|, \tag{4.5}$$

for RSPT3. This particular quantity is considered since it is directly comparable to the results of Fig. 4.4. Only a few select particle counts N are considered as computations in 80 HO basis functions are considerably slower. All in all, the convergence error due to basis size can be seen to be roughly one quarter of the error between the second and third order methods in Fig. 4.4. This indicates that not only is it necessary to go to higher perturbative orders to get more accurate results, but also to increase the basis size used.

Table 4.2: Absolute energy difference between 64 and 80 HO basis functions, computed using RSPT3 and ENPT3. See Eq. 4.5 for a definition of the quantity presented. Shown for particle counts $N = 4, 30, 100$.

		Abs. energy diff. (a. u. $\times 10^{-3}$)		
$\boldsymbol{\lambda}$	**Method**	$N = 4$	$N = 30$	$N = 100$
-0.5	RSPT3	0.241	0.178	0.173
	ENPT3	0.241	0.178	0.173
0.5	RSPT3	0.187	0.155	0.152
	ENPT3	0.188	0.155	0.152
-1.0	RSPT3	1.08	0.772	0.748
	ENPT3	1.09	0.772	0.748
1.0	RSPT3	0.651	0.581	0.573
	ENPT3	0.660	0.581	0.573

4.5 Scaling of many-body perturbation theory with interaction strength

Before wrapping up our analysis of the one-component GP equation, it is of interest to keep the particle count N fixed whilst the interaction strength g is varied. This aims to further explore the stability of the method and examine the behaviour of the perturbative methods as the size of the perturbation is increased. A few words of caution are in order as increasing the size of the perturbation obviously goes against the assumption that the perturbation is small, however what constitutes *small* is still up for debate and the goal of this exploration.

The left panel of Fig. 4.5 presents the relative energy difference between ENPT3 and the mean-field energy E_{GP} along with a zoomed in view to capture the behaviour at smaller energy scales. This time for a fixed particle count $N = 100$ and non-linear parameter in the range $\lambda = g(N-1) \in [-2, 2]$ as g is varied. In the same figure, the right panel shows the absolute energy difference between the first- and second order, and second- and third order perturbative methods. The left panel captures the importance of the MBPT methods and their impact on the total energy of the system, whilst the right panel shows the convergence of the individual MBPT methods with respect to order. Again, for all values of λ the BeMF system was solved self-consistently and the fractional occupation was computed to $n_0/N = 1$, meaning the GP ground state is accurate. As previously, 64 HO basis functions were used in the SCF and MBPT calculations.

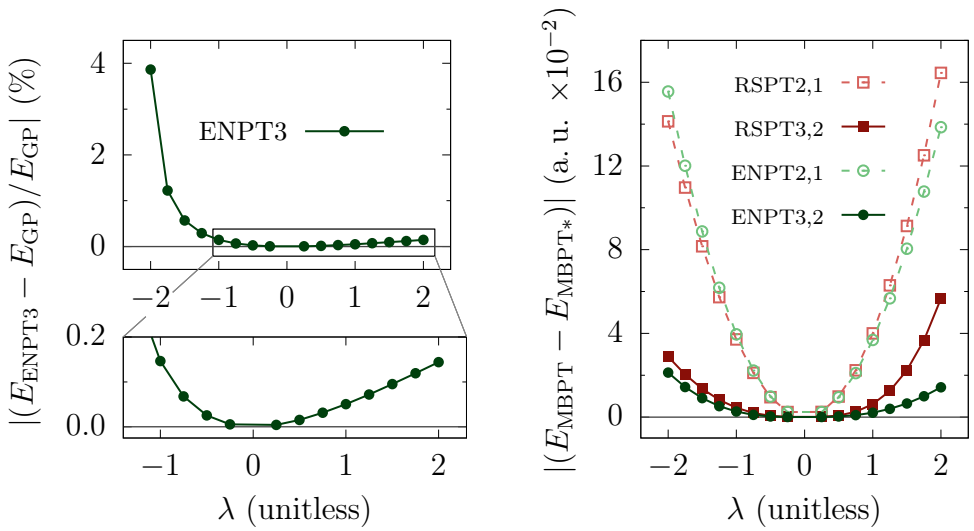

Figure 4.5: Relative energy difference of ENPT3 to the mean-field energy E_{GP} (left) with a zoomed in view to show behaviour for smaller energies. Along with the absolute energy difference between the first- and second order, and second- and third order MBPT methods (right). Both shown as a function of the non-linear parameter $\lambda = g(N-1)$ for a fixed particle count $N = 100$.

Immediately noteworthy in the left panel of Fig. 4.5 is the impact of the MBPT methods on BECs with attractive interactions $\lambda < 0$ compared to repulsive ones $\lambda > 0$. The overall size of the energy correction is roughly symmetric with respect to λ, but the lower mean-field energy in the attractive case results in a larger relative contribution from the corrections. From the right panel it is interesting to note the surprisingly good convergence behaviour of the MBPT methods with respect to perturbative order. Especially as the perturbation is by no means small, $\lambda = 1$ effectively equates the perturbation to the unperturbed Hamiltonian. Similarly to the previous section, we again see better convergence behaviour for ENPT with respect to perturbative order compared to RSPT.

Lastly, the convergence of the RSPT3 and ENPT3 methods is examined with respect to the basis size. Table 4.3 shows the absolute energy difference between 64 and 80 HO basis functions for each of the methods, and for a few select values of λ. See Eq. (4.5) for how to calculate this quantity. The presented errors have been rounded to three significant digits, and are not exactly equal between the methods if more digits were to be included. Yet again the error due to basis size is small compared to the error between the second- and third order methods in Fig. 4.5. Convergence with respect to basis size is also seen to worsen for larger $|\lambda|$ and particularly for $\lambda < 0$ corresponding to systems where beyond mean-field effects dominate.

Table 4.3: Absolute energy difference between 64 and 80 HO basis functions, computed using RSPT3 and ENPT3. See Eq. 4.5 for a definition of the quantity presented.

	Abs. energy diff. (a. u. $\times 10^{-2}$)	
$\boldsymbol{\lambda}$	**RSPT3**	**ENPT3**
-2	0.359	0.359
-1	0.0748	0.0748
1	0.0573	0.0573
2	0.208	0.208

4.6 Case studies of more complicated systems

With a thorough analysis of a one-component BEC in a harmonic trap completed, interest shifts towards systems that diverge from this path in some manner. This effort will be explored in two ways: firstly perturbing the harmonic potential via the introduction of a centered Gaussian, creating a double well, and secondly by studying a system where the beyond mean-field effects play a crucial role, the self-bound BEC droplet.

4.6.1 One-component Bose-Einstein condensate in a double well

Firstly, a quick motivation of the choice to study a BEC in a double well. Previous studies, both experimental and theoretical, on the dynamics of a BEC in a double well have concluded that for particle counts $N < N_c$ where N_c is some critical particle count, so called Josephson Oscillations occur where the BEC tunnels back and forth between the wells [56, 57]. Additionally for $N > N_c$ the BEC *self-traps* in one of the wells due to the strength of the inter-particle interactions [56, 57]. For these dynamically unstable states, the GP equation, which is a stationary equation, is known to break down and result in a ground state with broken symmetry compared to the Hamiltonian [35]. The question is then whether or not MBPT can restore the correct symmetry of the ground state.

We consider a one-component BEC modeled by the GP equation (2.14) with the trapping potential

$$u(x) = \frac{1}{2}x^2 + \frac{2}{\sigma\sqrt{2\pi}} \exp\left(-\frac{x^2}{2\sigma^2}\right), \qquad \sigma = 1/10, \tag{4.6}$$

consisting of a harmonic trap with a centered Gaussian. After solving this system self-consistently using $\lambda = -1$, two different ground states emerge depending on the initial guess. This is illustrated in Fig. 4.6 where the density per particle is plotted over space for a symmetric and asymmetric ground state, resulting from an initial guess with the same respective symmetry. Note that an asymmetric ground state focused on the right well may also be achieved by using an initial guess that shares this property. The energy for the two asymmetric states are the same and as such only one of them is shown for clarity. All computations were performed using 64 HO basis functions.

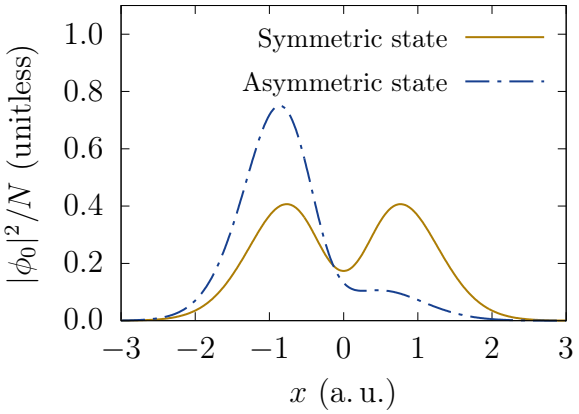

Figure 4.6: Density per particle over space for the two mean-field ground states of an attractive BEC ($\lambda = -1$) in a double well, the two states results from a symmetric and asymmetric guess respectively.

Before moving on to perturbation calculations, a few things will be said about why this sensitive dependence on initial guess occurs to begin with, since this behaviour was not seen when a purely harmonic trap was used. Looking at the mean-field energies per particle for the symmetric $E_{\text{sym}} \approx 0.9987$ a. u. and asymmetric $E_{\text{asym}} \approx 0.9820$ a. u. states reveals that they are almost degenerate and that the asymmetric state is the mean-field ground state. As to why a symmetric guess would converge to a state that is not the ground state comes down to the fact that if the initial guess $|\phi^{(0)}\rangle$ is symmetric then the contribution to the GP Hamiltonian $\lambda|\phi^{(0)}|^2$ will share this symmetry as will lowest energy state the next SCF iteration, and so on. This results in a final state that shares the symmetry of the initial guess.

Moving on to MBPT methods, Fig. 4.7 shows the mean-field and MBPT energies per particle as a function of particle count N in the mean-field limit (keeping $\lambda = -1$) for both the symmetric and asymmetric ground states. Both RSPT3 and ENPT3 are shown along with a shaded region around each line which represents the distance between the second- and third order methods. The BeMF calculations were also performed and the fractional occupations were calculated for multiple asymmetric and symmetric initial guesses, and no improvement upon the GP ground states were found. Computations were yet again performed using 64 HO basis functions.

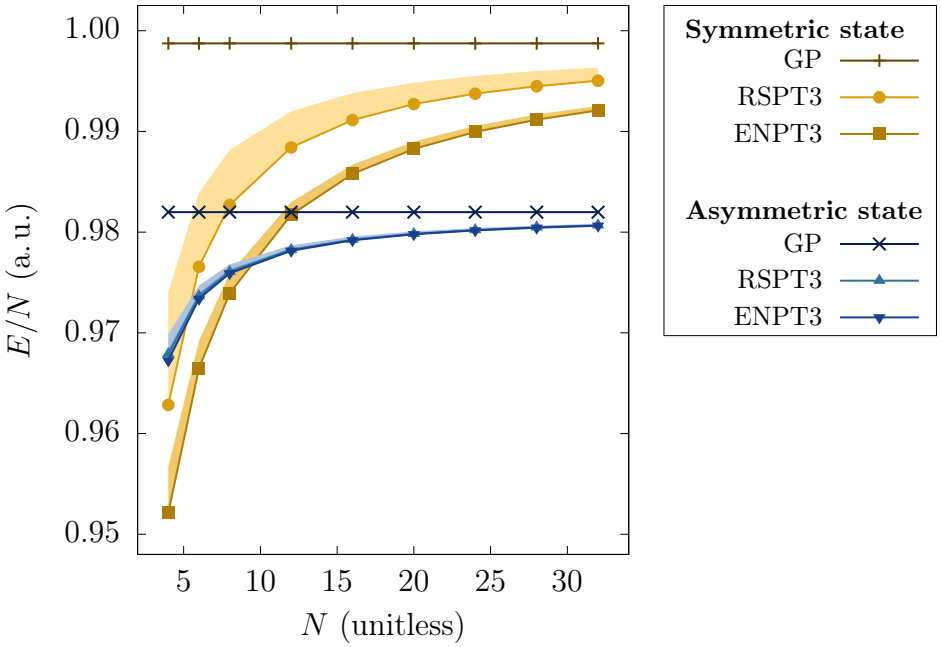

Figure 4.7: Third order RSPT and ENPT applied to the symmetric and asymmetric states in Fig. 4.6. Energies are shown per particle as a function of particle count N in the mean-field limit (keeping $\lambda = g(N-1) = -1$ constant). Mean-field (GP) energies are shown for reference and are constant as λ is kept fix. The shaded regions around RSPT3 and ENPT3 represents the difference between the second and third order methods.

Interestingly, when far away from the mean-field limit, that is for lower $4 \leq N \leq 8$, starting from the symmetric state yields lower energy ground states compared to starting from the asymmetric one. However, to actually ensure that the resulting ground states are symmetric for lower N, would require access to the perturbed wave functions, and is the topic of future studies. We can on the other hand hypothesize that if the perturbed state was asymmetric, then starting from an asymmetric mean-field state should have given a lower energy. As the particle count N is increased in the mean-field limit, RSPT3 and ENPT3 quickly converges towards their starting mean-field states, as expected, resulting in a ground state with broken symmetry once again.

Similarly to previous systems, ENPT3 yet again provides both a lower energy and presumably better accuracy compared to RSPT3. Qualitatively, it is safe to assume that RSPT has not converged with respect to perturbative order, and it seems necessary to go up to a higher order to get agreement between RSPT and ENPT. Lastly, regarding the convergence with respect to basis size, computations were made using 48 basis functions which resulted in slightly larger energies across the board, but the overall shape of Fig. 4.7 remained the same. We therefore assume that going to even higher basis sizes, although it will slightly improve the energies, will not change the large scale behaviour seen in the figure.

4.6.2 Self-bound two-component Bose-Einstein condensate in a weak harmonic trap

We start from a two-component BEC with contact interaction modeled by the GP equation (2.16) with symmetric intra-component interaction strengths $g = g_{AA} = g_{BB}$ and particle counts $N = N_A = N_B$, for each component. Specifically in the one-dimensional case, self-bound states have been found to form whenever intra-component interactions are repulsive $g > 0$ and inter-component interactions are attractive $g_{AB} < 0$, such that $g_{AB}^2 < g^2$ is satisfied [23, 58]. This inequality corresponds to the stable regime in the mean-field description where attractive beyond mean-field corrections were found to result in the formation of a self-bound droplet phase [23, 58]. Note that the GP equation by itself cannot model these self-bound states [23]. The ground state energy density $\mathcal{E} = E/L$ over a length L has analytically been found to be

$$\mathcal{E} = \delta g \eta^2 - \frac{4\sqrt{2}}{3\pi}(g\eta)^{3/2}, \tag{4.7}$$

where $\delta g = g_{AB} + \sqrt{g_{AA} g_{BB}} = g_{AB} + g$, and η is the number density $\eta = N/L$ in the volume V of a single component [58]. In particular we chose $g_{AB} = \gamma g$ for $\gamma \in [-1, 0]$ resulting in $\delta g = (1 + \gamma)g$.

Unfortunately, problems immediately arise in trying to replicate the above with our perturbative methods. In studying self-bound systems we want a trapping potential $u(x) = 0$, however the resultant system is not solvable self-consistently in the HO basis and our numerical integrals will fail to converge. Therefore we instead consider a weakly trapped condensate with $u(x) = \frac{1}{2}\omega x^2$ for a small oscillator strength ω. Note that the same ω is used in the definition of the HO eigenfunctions $\chi_n(x)$ in Eq. (4.1). Another problem that crops up is that a smaller ω corresponds to a wider potential well where the one-body eigenstates are much close in energy; Because of this, the SCF method will run into convergence issues for small enough ω. To figure out the smallest possible ω for which the SCF method converges, a two-component BEC was studied self-consistently with $N = 4$ particles and 48 HO basis functions for each component, safely within the stable regime with $g = 0.5/99$ and $g_{AB} = \gamma g$ with $\gamma = -0.90$. For this system, a smallest value of $\omega = 0.005$ was found to be stable, which will be used moving forward.

Next, the same system was studied for multiple $\gamma = -0.90, -0.95, -0.99$ and for particle counts $N \in [4, 60]$. Note that keeping g, g_{AB} fixed whilst increasing the particle count N will correspond to increasing the particle density η, as all particles in the condensate will interact will all other with the same interaction strength, which is only possible in a high density regime. Contrast this to the GP limit where the interaction strength between particles is decreased as the particle number increases, resulting in a very dilute condensate. The results are presented in Fig. 4.8 where the ground state energy per particle is shown for third order RSPT and ENPT, as a function of η. The shaded regions around each line again represents the energy difference between the second and third order for a given method. We estimated the number density via the mean-field wave wave function $\eta = N|\phi_0(0)|^2$. This estimate is reasonable as the resulting droplet state is expected to have a constant number density in the interior of the droplet. Also included in the figure are the analytical results calculated via Eq. (4.7), these values have been translated in energy by $\approx 2.44 \times 10^{-3}$ a. u. to allow for easier comparison to our MBPT results.

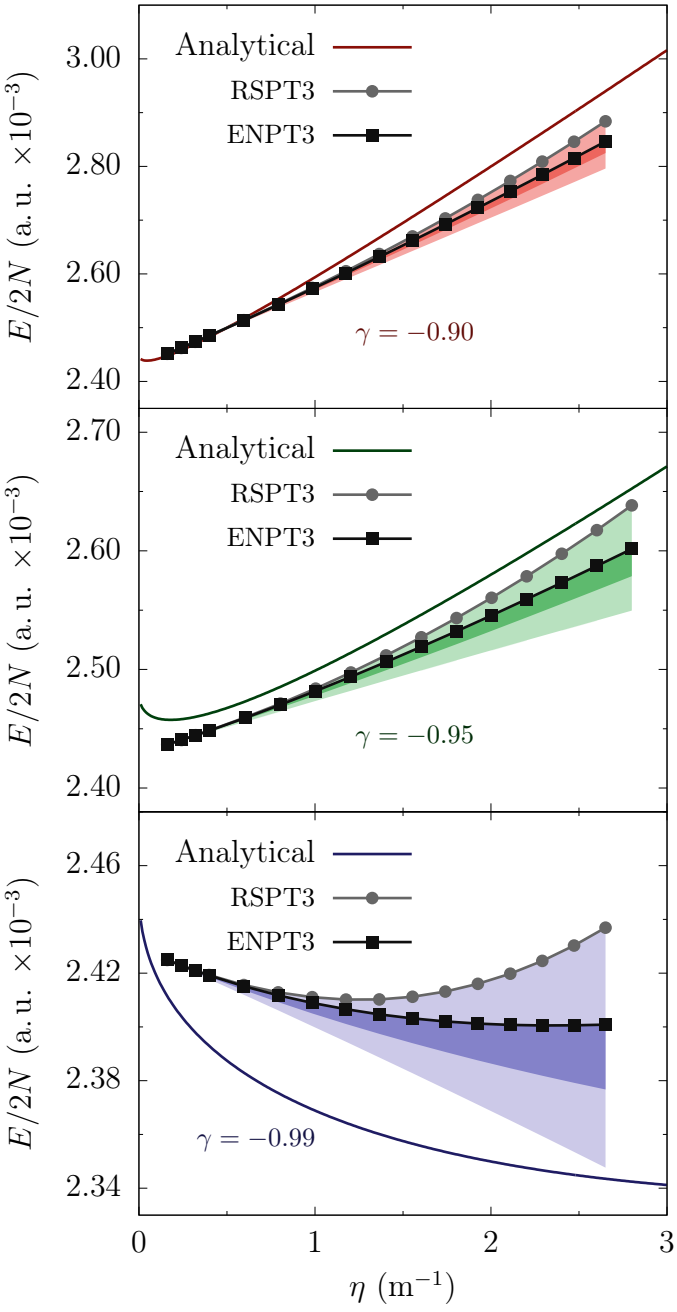

Figure 4.8: Ground state energy per particle of a two-component BEC, computed using third order RSPT and ENPT, all as a function of number density η. An intra-component interaction strength of $g = 0.5/99$ is considered for multiple inter-component interaction strengths $g_{AB} = \gamma g$, for $\gamma = -0.90$ (bottom), $\gamma = -0.95$ (middle), $\gamma = -0.99$ (top). The shaded regions around each line represents the energy difference between the second and third order for a given method. Analytical results from Ref. [58] are provided for reference and are translated in energy to match our MBPT methods.

Firstly, the overall shape of energy with respect to number density η in Fig. 4.8 appears to match what is expected for each γ. Unfortunately, our MBPT methods were either not able to correctly reproduce the analytically expected energy minima for $\gamma = -0.90, -0.95$, or they produced minima at the wrong number density η. To expand on the latter, for $\gamma = -0.99$, RSPT found a minimum at $\eta \approx 1.2$ and ENPT and at $\eta \approx 2.3$ whereas the expected minimum occurs for $\eta \approx 4.5$. This can partly be explained by our estimate of η from the mean-field wave function, and it would be interesting to see whether or not the situation could be improved with access to the perturbed wave function. Another reason for the discrepancy in the size and shape of the minima could be the presence of the external potential, the impact of which is hard to predict. For $\gamma = -0.90, -0.95$ the minima occur for very low η and might be visible if we extend the MBPT methods to account for $N < 4$, or rescale our system parameters such that the minima would occur for higher η. To the next question, why are our MBPT energies shifted by ≈ 2.45 a. u. ? Analytically one would expect $E = 0$ for $\eta = 0$, remember the analytical values were shifted for easier comparison. This shift is assumed to originate from to the presence of the weak trapping potential with $\omega = 0.005$ which lifts our ground state to higher energies. This is yet another reason as to why it would interesting to explore weaker potentials.

In comparing the MBPT methods we observe a similar behavior to the previously studied systems. That is ENPT3 produces lower energies with better accuracy compared to RSPT3. Additionally, the absolute energy difference between the second- and third order methods increase with N, which corresponds to a larger perturbation size as g, g_{AB} are kept fixed, which was also seen previously.

We lastly want to emphasize that these computations have been done in a relatively small basis of 48 HO basis functions, which is especially small considering $\omega = 0.005$ which corresponds to lots of energetically close mean-field states. The small basis was necessary to achieve reasonable computation times for the SCF method which required Hamiltonian mixing of $\alpha = 0.97$ for accurate results. We performed computations for 64 basis functions for $\gamma = -0.99$ and select values of $\eta \approx 0.16, 1.18, 2.228$ and found absolute errors in ENPT3 of size 0.0013×10^{-3}, 0.083×10^{-3}, and 0.37×10^{-3} a. u. respectively. For reference the absolute error between second- and third order ENPT for the same η was found to be 0.00057×10^{-3}, 0.33×10^{-3}, and 2.2×10^{-3} a. u. respectively. From this we can conclude that larger basis sizes are of primary interest for lower η whereas errors in the perturbative methods appears to dominate for larger η.

Chapter 5

Conclusion

To summarize, we have developed, implemented, and verified a perturbative approach to go beyond the mean-field description of a Bose-Einstein Condensate (BEC) provided by the Gross-Pitaevskii (GP) equation. This firstly required the implementation and verification of a Self-Consistent Field (SCF) method to find the one-body eigenstates and eigenvalues of the GP equation upon which the perturbation calculations could be made. Moreover, a so-called Best Mean-Field (BeMF) approach, where a fraction of the particles in the condensate were allowed in a state other than the ground state, was employed to ensure the accuracy of the GP ground state in cases where comparison to Full Configuration Interaction (FCI) were unfeasible. We considered one-dimensional condensates and worked in the Harmonic Oscillator (HO) basis.

The implemented SCF method correctly solved the non-linear GP and BeMF equations, and in cases where instabilities occur, Hamiltonian and orbital mixing were explored as potential remedies. Hamiltonian mixing proved fruitful in improving convergence for larger interaction strengths whilst orbital mixing remained unstable. Next, building upon the one-body states produced by the SCF method, two approaches to Many-Body Perturbation Theory (MBPT) were explored. The first method, a bosonic analogue to Møller-Plesset, here labeled Rayleigh-Schrödinger Perturbation Theory (RSPT) treating the many-body mean-field Hamiltonian $\hat{H}_{\mathrm{MF}} = \sum_{i=1}^{N} \hat{h}_{\mathrm{MF}}(x)$ for N particles as the unperturbed system. Meanwhile the second method relied on the partitioning of Epstein-Nesbet and was labeled ENPT.

The first system to be explored perturbatively was a one-component BEC in a harmonic trap. In the low particle number regime, calculated ground state energies could be compared to exact FCI energies for a given basis size. Both the third order RSPT and ENPT methods showed promising results, agreeing with FCI within a relative error of 1.5 ‰. However third order ENPT was found to consistently provide lower energies compared to third order RSPT. This was explained by the more accurate weighting of the matrix elements in the perturbative series of ENPT compared to RSPT. That being said, both methods showed a relatively large discrepancy between their second- and third order, indicating that higher order corrections may be of significance.

For the same system, scaling of the particle count N was explored in the mean-field limit, and agreement with the mean-field energy was found in the high particle number regime, as expected. Furthermore, scaling was also studied with respect to $\lambda = g(N-1)$ for a fixed particle count N. The MBPT methods were found to play an increasingly important role for $\lambda < 0$ compared to $\lambda > 0$, since the size of the beyond mean-field corrections is roughly symmetric with respect to the sign of λ, but the overall mean-field

energy is lower in the attractive case. Additionally, convergence of the RSPT and ENPT methods with respect to both perturbative order and basis size was explored in the above cases. The estimated error of the methods with respect to perturbative order (for a fixed basis size) was found to decrease with N and increase with $\lambda = g(N-1)$. The ENPT method consistently showed lower convergence errors with respect to order compared to the RSPT method. On the other hand, convergence with basis size did not differ between the methods. Both convergence types worsened for systems where beyond mean-field effects played a larger role, meaning for small N, larger λ and particularly $\lambda < 0$. An important take-away from this is that going to higher perturbative orders to improve the accuracy of the methods also necessitates larger basis sizes.

Next, we applied the MBPT methods to more complicated systems, albeit with moderate success. Firstly, a one-component BEC in a double well, and secondly a self-bound two-component BEC droplet were investigated. For the BEC in a double well, the mean-field ground state is known to exhibit breaking of symmetry with respect to the symmetry of the underlying potential. ENPT starting from a symmetric state mean-field ground state resulted in lower energies for small enough particle counts. Whether or not this state is symmetric was left unknown since we did not have access to the perturbed wave functions. It is however reasonable to expect that if the perturbed state was asymmetric, then starting from an asymmetric mean-field state should have given a lower energy, which it did not. Lastly, the possibility of describing self-bound two-component BEC droplets which rely heavily on beyond mean-field effects to stabilize, was explored. Our methods managed to capture the overall shape of the condensate energy with respect to number density. They, however, failed to describe the characteristic energy minima one would analytically expect. Reasons for this are hypothesized to be many, including too small of a basis set, wrong type of basis set, or the presence of an external potential. This external potential, albeit weak, was required for the SCF method to converge in the HO basis. The effects of this potential on the ground state energy, could however drown out the delicate interactions necessary for the formation of a self-bound state. Our results are a good indicator that perturbative methods could indeed describe these self-bound states; further studies are necessary. For both the double well and self-bound systems ENPT performed better compared to RSPT, resulting both in lower energies but also better convergence with respect to perturbative order. This is in agreement with our observations of the simpler harmonically trapped condensates.

Chapter 6

Outlook

With the perturbative beyond mean-field methods developed and verified, the question of how to proceed naturally arises, and the answers are many. Extensions could be made of the method itself to allow for higher order perturbations to better verify the accuracy of the methods. It would then be interesting to see whether or not the agreement between RSPT and ENPT could be improved, particularly for larger interaction strengths and non-linear parameters. This would in turn require larger basis sizes and thus requires further optimizations on the implementation side. On the topic of perturbation theory, having access to the perturbed wave functions in addition to the energies would be important when studying the physics of all of these systems.

Moreover, other avenues of extensions include increasing the dimensionality to two or three dimensions which primarily involves swapping out the numerical integration routines and restructuring the code to work on vectors. Concerning a restructuring of the code, the computation of perturbations as it stands are ripe for further parallelization and porting more of the code to run on a GPU for instance would not be too much trouble. This could then in turn allow for the efficient study of systems with larger basis sizes, which would be necessary for higher order perturbation theory. This work serves as an excellent benchmarking tool in the further implementation and exploration of more complicated beyond mean-field methods for bosonic systems.

Since this thesis has been focused primarily on systems with contact interaction, it would be interesting to apply these MBPT methods to systems with long range dipolar interactions, which would allow for the study of one-component self-bound dipolar droplets as well. Further exploration of these methods in the study of two-component droplets with contact interaction is also possible. It would be particularly interesting to apply perturbation theory to the extended GP equation, which already takes some beyond mean-field effects into account, and would thus constitute a better starting point in the study of droplets [23]. Moreover, to explore weaker trapping potentials it would be a good idea to use a more appropriate basis, such as the Fourier basis consisting of sines and cosines, or possibly even B-splines. We note however that the study of three-dimensional droplets is not possible with the present approach as we require a stable mean-field solution as a starting point, and the three-dimensional droplet is known to form only in the unstable regime (see Refs. [23] & [58]). Two-dimensional droplets on the other hand also form in the stable regime and might therefore be of interest for future studies [23, 58].

Appendices

Appendix A

The mathematics of second quantization

We start from the time-independent one-body Schrödinger equation (2.2), where solutions are sought after in the Hilbert space $|\phi_n\rangle \in \mathcal{H}$ with inner product $\langle\cdot|\cdot\rangle_{\mathcal{H}}$. Then the many-body Hilbert space containing a system of N particles may be constructed as

$$\mathcal{H}^{\otimes N} = \underbrace{\mathcal{H} \otimes \mathcal{H} \otimes \cdots \otimes \mathcal{H}}_{N \text{ products}}, \tag{A.1}$$

where "$\otimes$" denotes the tensor product, and the inner product in $\mathcal{H}^{\otimes N}$ is inherited from $\mathcal{H}$ as

$$\langle\cdot|\cdot\rangle_{\mathcal{H}^{\otimes N}} = \prod_{i=1}^{N} \langle\cdot|\cdot\rangle_{\mathcal{H}}. \tag{A.2}$$

An example of an element in this space is $|\phi_i\phi_j\rangle = |\phi_i\rangle \otimes |\phi_j\rangle \in \mathcal{H}^{\otimes 2}$ where one particle resides in $|\phi_i\rangle$ and one in $|\phi_j\rangle$, note that particles in this space are distinguishable as the inner product between $|\phi_i\phi_j\rangle$ and $|\phi_j\phi_i\rangle$ is $\langle\phi_i\phi_j|\phi_j\phi_i\rangle_{\mathcal{H}^{\otimes 2}} = 0, i \neq j$, which is not suitable for describing bosonic or fermionic systems. To solve this one considers the symmetric or antisymmetric subspace of $\mathcal{H}^{\otimes N}$ with respect to particle interchange often denoted via the symmetrization (antisymmetrization) operator $\hat{S}$ ($\hat{A}$) as $\hat{S}\mathcal{H}^{\otimes N}$ ($\hat{A}\mathcal{H}^{\otimes N}$) [59, 60]. For instance $\hat{S}\mathcal{H}^{\otimes 2}$ then contains states $|\phi_i\phi_j\rangle = \frac{1}{\sqrt{2}}(|\phi_i\phi_j\rangle + |\phi_j\phi_i\rangle), i \neq j$ and the expected the inner product is restored $\langle\phi_i\phi_j|\phi_j\phi_i\rangle_{\hat{S}\mathcal{H}^{\otimes 2}} = 1$. Moreover, if $N = 0$ the *empty* space is defined as some field $\mathcal{H}^{\otimes 0} = \mathbb{C}$, most commonly the complex numbers [59].

The many-body spaces $\mathcal{H}^{\otimes N}$ may be used to construct the so called Fock space $\mathcal{F}(\mathcal{H})$ which encompasses all many-body spaces of differing particle counts N. The construction of the Fock space is a formal sum over all many-body spaces

$$\mathcal{F}(\mathcal{H}) = \bigoplus_{n=0}^{\infty} \mathcal{H}^{\otimes n}, \tag{A.3}$$

and its structure may intuitively be understood as an infinite non-commutative polynomial with $\mathcal{H}$ as a formal variable, for instance $\mathbb{C} \oplus \mathcal{H} \oplus (\mathcal{H} \otimes \mathcal{H}) \in \mathcal{F}(\mathcal{H})$ and is vaguely analogous to a polynomial $f(x) = k + x + x^2, \quad k \in \mathbb{C}$ [59, 60]. Similarly, the symmetric and antisymmetric Fock spaces $\mathcal{F}_s(\mathcal{H})$ and $\mathcal{F}_a(\mathcal{H})$ are constructed by instead summing

over $\hat{S}\mathcal{H}^{\otimes N}$ and $\hat{A}\mathcal{H}^{\otimes N}$.

A particularly important element of $\mathcal{F}(\mathcal{H})$ is the vacuum state $|0\rangle = 1 \in \mathbb{C}$ containing no particles. Yet again it is possible to define an inner product on $\mathcal{F}(\mathcal{H})$ as

$$\langle \cdot | \cdot \rangle_{\mathcal{F}(\mathcal{H})} = \sum_{n=0}^{\infty} \langle \cdot | \cdot \rangle_{\mathcal{H}^{\otimes n}}. \tag{A.4}$$

For the proof of completeness of $\mathcal{F}(\mathcal{H})$ see Ref. [59]. Focusing on the bosonic Fock space $\mathcal{F}_s(\mathcal{H})$ moving forward, an example of an inner product in this space between $|\phi_0\phi_0\rangle$ and $|\phi_0\phi_1\rangle$ is calculated as

$$\langle \phi_0\phi_0 | \phi_0\phi_1 \rangle_{\mathcal{F}_s(\mathcal{H})} = \langle \phi_0\phi_0 | \phi_0\phi_1 \rangle_{\hat{S}\mathcal{H}^{\otimes 2}} = \langle \phi_0 | \phi_0 \rangle_{\mathcal{H}} \frac{1}{\sqrt{2}} (\langle \phi_0 | \phi_1 \rangle_{\mathcal{H}} + \langle \phi_1 | \phi_0 \rangle_{\mathcal{H}}) = 0. \tag{A.5}$$

Similarly the inner product is also zero if the states contain a different amount of particles since the many-body spaces of different N are orthogonal [59]. In general the inner product between two elements of $\mathcal{F}_s(\mathcal{H})$ is only non-zero if they both contain the same elements of $\mathcal{H}$ with the same occupations. Usually the occupation number notation is preferred where for example a many-body state consisting of one-body states $|\phi_0\rangle, |\phi_1\rangle, |\phi_2\rangle$ where two particles reside in $|\phi_1\rangle$, and one in $|\phi_2\rangle$, is written as $|0, 2, 1\rangle$.

Equipped with the notion of a bosonic Fock space $\mathcal{F}_s(\mathcal{H})$ linking together all different many-body spaces $\hat{S}\mathcal{H}^{\otimes N}$ it is possible to define the bosonic creation and annihilation operators $\hat{a}^\dagger$ and $\hat{a}$ linking spaces of N to spaces of $N \pm 1$ particles

$$\hat{a}^\dagger : \hat{S}\mathcal{H}^{\otimes N} \to \hat{S}\mathcal{H}^{\otimes N+1} \tag{A.6}$$

$$\hat{a} : \hat{S}\mathcal{H}^{\otimes N} \to \hat{S}\mathcal{H}^{\otimes N-1} \tag{A.7}$$

with the action that $\hat{a}_i^\dagger$ creates and $\hat{a}_i$ destroys a particle in state ϕ_i. As an example consider $|\ldots, n_{i-1}, n_i, n_{i+1}, \ldots\rangle$ with n_i particles in state ϕ_i, then

$$\hat{a}_i^\dagger | \ldots, n_{i-1}, n_i, n_{i+1}, \ldots \rangle = \sqrt{n_i + 1} | \ldots, n_{i-1}, n_i + 1, n_{i+1}, \ldots \rangle \tag{A.8}$$

$$\hat{a}_i | \ldots, n_{i-1}, n_i, n_{i+1}, \ldots \rangle = \sqrt{n_i} | \ldots, n_{i-1}, n_i - 1, n_{i+1}, \ldots \rangle. \tag{A.9}$$

Moreover, acting on the vacuum state with a annihilation operator destroys the state, that is $\hat{a}|0\rangle = 0|0\rangle = 0$ [11]. It is also important to mention the commutation relations of the bosonic creation and annihilation operators

$$\left[\hat{a}_i, \hat{a}_j\right] = 0, \quad \left[\hat{a}_i^\dagger, \hat{a}_j^\dagger\right] = 0, \quad \left[\hat{a}_i, \hat{a}_j^\dagger\right] = \delta_{ij}, \tag{A.10}$$

where δ_{ij} is the Kronecker delta [11].

Building on the creation and annihilation operators, it is now possible to construct any symmetric many-body state in $\mathcal{F}_s(\mathcal{H})$ by acting on $|0\rangle$. If a system consists of M different states labeled by $\{|\phi_i\rangle\}$, $\quad i = 0, \ldots, M-1$ with n_i bosons in each state, then the full many-body state may be comfortably constructed as [11]

$$|\Psi\rangle = |n_1, n_2, \ldots\rangle = \prod_{i=0}^{M-1} \frac{(\hat{a}_i^\dagger)^{n_i}}{\sqrt{n_i!}} |0\rangle. \tag{A.11}$$

It is then possible to express many-body operators $\hat{H} = \sum_{i=1}^{N} \hat{h}(x_i)$ constructed from a single-particle operator $\hat{h}(x)$ in terms of the creation and annihilation operators $\hat{a}^\dagger$ and $\hat{a}$ [11]. The operator becomes

$$\hat{H} = \sum_{ij} h_{ij} \hat{a}_i^\dagger \hat{a}_j, \tag{A.12}$$

where the sum runs over $i, j = 0, 1, \ldots, \infty$ and [11]

$$h_{ij} = \int \mathrm{d}x \, \phi_i^*(x) \hat{h}(x) \phi_j(x). \tag{A.13}$$

Similarly, for many-body two-particle operators $\hat{V} = \sum_{i<j}^{N} \hat{v}(x_i, x_j)$ one gets

$$\hat{V} = \frac{1}{2} \sum_{ijkl} v_{ijkl} \hat{a}_i^\dagger \hat{a}_j^\dagger \hat{a}_l \hat{a}_k, \tag{A.14}$$

where the sum runs over $i, j, k, l = 0, 1, \ldots, \infty$ and [11]

$$v_{ijkl} = \int \mathrm{d}x \int \mathrm{d}x' \, \phi_i^*(x) \phi_j^*(x') \hat{v}(x, x') \phi_k(x) \phi_l(x'). \tag{A.15}$$

Finally, the theory is easily extend to describe a system of different species of bosons. Assuming the species are chemically independent, each component of the system may be labeled by $A, B, \ldots$ and assigned its own Fock space $\mathcal{F}_s^{(A)}(\mathcal{H}), \mathcal{F}_s^{(B)}(\mathcal{H}), \ldots$; Then the many-component Fock space is constructed as $\mathcal{F}_s^{(A)}(\mathcal{H}) \otimes \mathcal{F}_s^{(B)}(\mathcal{H}) \otimes \ldots$ with the inner product

$$\langle \cdot | \cdot \rangle_{\mathcal{F}_s^{(A)}(\mathcal{H}) \otimes \mathcal{F}_s^{(B)}(\mathcal{H}) \otimes \ldots} = \prod_{I \in \{A, B, \ldots\}} \langle \cdot | \cdot \rangle_{\mathcal{F}_s^{(I)}(\mathcal{H})}, \tag{A.16}$$

which is only non-zero when the many-component states contain the same components and the same many-body states within those components.

Consider two components A and B with N_A particles in A and N_B particles in B, a two-particle operator can be written as $\hat{V} = \sum_{i=1}^{N_A} \sum_{j=1}^{N_B} \hat{v}(x_i^{(A)}, x_j^{(B)})$. Expressing this operator in terms of creation and annihilation operators results in

$$\hat{V} = \sum_{ijkl} v_{ijkl}^{(AB)} \hat{a}_{A_i}^\dagger \hat{a}_{B_j}^\dagger \hat{a}_{B_l} \hat{a}_{A_k}, \tag{A.17}$$

where

$$v_{ijkl}^{(AB)} = \int \mathrm{d}x \int \mathrm{d}x' \, \phi_{A_i}^*(x) \phi_{B_j}^*(x') \hat{v}(x, x') \phi_{A_k}(x) \phi_{B_l}(x'). \tag{A.18}$$

This requires taking into account the conservation of particle counts N_A, N_B and the fact that integrals over wave functions associated with different species of bosons is zero.

Appendix B

Matrix elements needed for third order perturbation theory

In calculating the third order energy shift to the ground state of a two-component BEC modeled by the GP equation, matrix elements $\langle\Psi_k^{(0)}|\hat{V}|\Psi_{k'}^{(0)}\rangle$ between two double substitution states $|\Psi_k^{(0)}\rangle, |\Psi_{k'}^{(0)}\rangle \in \mathcal{F}_s^{(AB)}(\mathcal{H})$, needs to be evaluated. Here $\hat{V}$ is the perturbation given by Eq. (3.5) and the double substitutions are expressed in the notation presented in Eq. (3.13). Starting with the case where $|\Psi_k^{(0)}\rangle = |\Psi_{k'}^{(0)}\rangle$, and if both excitations reside in the same one-body state $|\phi_{A_m}\rangle$ then

$$
\begin{aligned}
\langle A_m A_m|\hat{V}|A_m A_m\rangle = \frac{1}{2}g_{AA}\Big(&2v_{mmmm}^{(AA)} + 8(N_A-2)v_{m0m0}^{(AA)} \\
&+(N_A-2)(N_A-3)v_{0000}^{(AA)}\Big) \\
&- g_{AA}(N_A-1)\left(2v_{m0m0}^{(AA)} + (N_A-2)v_{0000}^{(AA)}\right) \\
&+ \frac{1}{2}g_{BB}N_B(N_B-1)v_{0000}^{(BB)} - g_{BB}(N_B-1)N_B v_{0000}^{(BB)} \\
&+ g_{AB}N_B\left((N_A-2)v_{0000}^{(AB)} + 2v_{m0m0}^{(AB)}\right) \\
&- g_{AB}N_B\left((N_A-2)v_{0000}^{(AB)} + 2v_{m0m0}^{(AB)}\right) \\
&- g_{AB}N_A N_B v_{0000}^{(BA)} \\
= \frac{1}{2}g_{AA}\Big(&2v_{mmmm}^{(AA)} + 8(N_A-2)v_{m0m0}^{(AA)} \\
&+(N_A-2)(N_A-3)v_{0000}^{(AA)}\Big) \\
&- g_{AA}(N_A-1)\left(2v_{m0m0}^{(AA)} + (N_A-2)v_{0000}^{(AA)}\right) \\
&- g_{AB}N_A N_B v_{0000}^{(BA)},
\end{aligned}
\tag{B.1}
$$

where $v_{ijkl}^{(PQ)}$ are the integrals in Eq. (2.9). Secondly, if the excitations instead reside in two different one-body states $|\phi_{A_m}\rangle$ and $|\phi_{A_n}\rangle$ where $m \neq n$ we get

$$\begin{aligned}
\langle A_m A_n|\hat{V}|A_m A_n\rangle &= \frac{1}{2}g_{AA}\Big(4v_{mnmn}^{(AA)} + 4(N_A-2)v_{m0m0}^{(AA)} + 4(N_A-2)v_{n0n0}^{(AA)} \\
&\qquad + (N_A-2)(N_A-3)v_{0000}^{(AA)}\Big) \\
&\quad - g_{AA}(N_A-1)\left(v_{m0m0}^{(AA)} + v_{n0n0}^{(AA)} + (N_A-2)v_{0000}^{(AA)}\right) \\
&\quad + \frac{1}{2}g_{BB}N_B(N_B-1)v_{0000}^{(BB)} - g_{BB}(N_B-1)N_B v_{0000}^{(BB)} \\
&\quad + g_{AB}N_B\left((N_A-2)v_{0000}^{(AB)} + v_{m0m0}^{(AB)} + v_{n0n0}^{(AB)}\right) \\
&\quad - g_{AB}N_B\left((N_A-2)v_{0000}^{(AB)} + v_{m0m0}^{(AB)} + v_{n0n0}^{(AA)}\right) \\
&\quad - g_{AB}N_A N_B v_{0000}^{(BA)} \\
&= \frac{1}{2}g_{AA}\Big(4v_{mnmn}^{(AA)} + 4(N_A-2)v_{m0m0}^{(AA)} + 4(N_A-2)v_{n0n0}^{(AA)} \\
&\qquad + (N_A-2)(N_A-3)v_{0000}^{(AA)}\Big) \\
&\quad - g_{AA}(N_A-1)\left(v_{m0m0}^{(AA)} + v_{n0n0}^{(AA)} + (N_A-2)v_{0000}^{(AA)}\right) \\
&\quad - g_{AB}N_A N_B v_{0000}^{(BA)}.
\end{aligned} \tag{B.2}$$

Thirdly, if $|\Psi_k^{(0)}\rangle$ and $|\Psi_{k'}^{(0)}\rangle$ only differ in one excited state

$$\begin{aligned}
\langle A_m A_m|\hat{V}|A_m A_p\rangle &= \frac{1}{2}g_{AA}\left(4\sqrt{2}(N_A-2)v_{m0p0}^{(AA)} + 2\sqrt{2}v_{mmmp}^{(AA)}\right) \\
&\quad - g_{AA}(N_A-1)\sqrt{2}v_{m0p0}^{(AA)} \\
&\quad + g_{AB}N_B v_{m0p0}^{(AB)} - g_{AB}N_B v_{m0p0}^{(AB)} \\
&= g_{AA}\left((N_A-3)\sqrt{2}v_{m0p0}^{(AA)} + \sqrt{2}v_{mmmp}^{(AA)}\right),
\end{aligned} \tag{B.3}$$

or $|\Psi_k^{(0)}\rangle$ and $|\Psi_{k'}^{(0)}\rangle$ are allowed to differ in two excited states, then more possibilities open up

$$\langle A_m A_m|\hat{V}|A_p A_p\rangle = \frac{1}{2} g_{AA} 2 v_{mmpp}^{(AA)} = g_{AA} v_{mmpp}^{(AA)}, \tag{B.4}$$

$$\langle A_m A_m|\hat{V}|A_p A_q\rangle = \frac{1}{2} g_{AA} 2\sqrt{2} v_{mmpq}^{(AA)} = \sqrt{2} g_{AA} v_{mmpq}^{(AA)}, \tag{B.5}$$

$$\begin{aligned}\langle A_m A_n|\hat{V}|A_m A_q\rangle &= \frac{1}{2} g_{AA} \left(4(N_A-2) v_{0n0q}^{(AA)} + 4 v_{mnmq}^{(AA)}\right) - g_{AA}(N_A-1) v_{0n0q}^{(AA)} \\ &\quad + g_{AB} N_B v_{n0q0}^{(AB)} - g_{AB} N_B v_{n0q0}^{(AB)} \\ &= g_{AA}\left((N_A-3) v_{0n0q}^{(AA)} + 2 v_{mnmq}^{(AB)}\right),\end{aligned} \tag{B.6}$$

$$\langle A_m A_n|\hat{V}|A_p A_q\rangle = \frac{1}{2} g_{AA} 4 v_{mnpq}^{(AA)} = 2 g_{AA} v_{mnpq}^{(AA)}. \tag{B.7}$$

Lastly if an excitation occurs in each component and we require that $|\Psi_k^{(0)}\rangle = |\Psi_{k'}^{(0)}\rangle$, then the possible matrix element becomes

$$\begin{aligned}\langle A_m B_n|\hat{V}|A_m B_n\rangle &= \frac{1}{2} g_{AA}\left((N_A-1)(N_A-2) v_{0000}^{(AA)} + 4(N_A-1) v_{m0m0}^{(AA)}\right) \\ &\quad - g_{AA}(N_A-1)\left((N_A-1) v_{0000}^{(AA)} + v_{m0m0}^{(AA)}\right) \\ &\quad + \frac{1}{2} g_{BB}\left((N_B-1)(N_B-2) v_{0000}^{(BB)} + 4(N_B-1) v_{n0n0}^{(BB)}\right) \\ &\quad - g_{BB}(N_B-1)\left((N_B-1) v_{0000}^{(BB)} + v_{n0n0}^{(BB)}\right) \\ &\quad + g_{AB}\Big((N_A-1)(N_B-1) v_{0000}^{(AB)} + (N_A-1) v_{0n0n}^{(AB)} \\ &\qquad\qquad + (N_B-1) v_{m0m0}^{(AB)} + v_{mnmn}^{(AB)}\Big) \\ &\quad - g_{AB} N_B\left((N_A-1) v_{0000}^{(AB)} + v_{m0m0}^{(AB)}\right) \\ &\quad - g_{AB} N_A N_B\left((N_B-1) v_{0000}^{(AB)} + v_{0n0n}^{(AB)}\right) \\ &= \frac{1}{2} g_{AA}\left(-N_A(N_A-1) v_{0000}^{(AA)} + 2(N_A-1) v_{m0m0}^{(AA)}\right) \\ &\quad + \frac{1}{2} g_{BB}\left(-N_B(N_B-1) v_{0000}^{(BB)} + 2(N_B-1) v_{n0n0}^{(BB)}\right) \\ &\quad + g_{AB}\left((1-N_A N_B) v_{0000}^{(AB)} - v_{0n0n}^{(AB)} - v_{m0m0}^{(AB)} + v_{mnmn}^{(AB)}\right).\end{aligned} \tag{B.8}$$

Similarly if $|\Psi_k^{(0)}\rangle$ and $|\Psi_{k'}^{(0)}\rangle$ then differ in one excited state

$$\begin{aligned}\langle A_m B_n|\hat{V}|A_m B_p\rangle &= \frac{1}{2} g_{BB}\left(4(N_B-1)v_{n0p0}^{(BB)}\right) - g_{BB}(N_B-1)v_{n0p0}^{(BB)} \\ &\quad + g_{AB}\left((N_A-1)v_{0n0p}^{(AB)} + v_{mnmp}^{(AB)}\right) - g_{AB}N_A v_{0n0p}^{(AB)} \\ &= g_{BB}(N_B-1)v_{0n0p}^{(BB)} + g_{AB}(v_{mnmp}^{(AB)} - v_{0n0p}^{(AB)}),\end{aligned} \tag{B.9}$$

or two excited states

$$\langle A_m B_n|\hat{V}|A_p B_q\rangle = g_{AB} v_{mnpq}^{(AB)}. \tag{B.10}$$

This concludes the calculation of all matrix elements between two double substitutions, which are necessary for third order perturbation theory.

Appendix C

Pseudo-code implementation of Rayleigh-Schrödinger perturbation theory applied to the one-component Gross-Pitaevskii equation

Diving right in, Algorithm 1 shows a pseudo-code implementation of the RSPT calculations as applied to the GP equations, precisely as described in Section 3.1. As input, a set of solutions $\{|\phi_i\rangle\}$, $\{\mu_i\}$, $i \in [0, M-1]$ to the original GP problem given by Eq. (2.14), and as output the beyond mean-field energy calculated perturbatively to order three. More in depth, equations (3.7), (3.8), (3.17) and (3.18) are used to calculated the energy shifts of order 0,1,2, and 3 respectively. Moreover, the fixed size array t refers to a caching of terms given by Eq. (3.19) to avoid as many inner product calculations as possible, and v_{ijkl} refers to the integrals over the input orbitals (see Eq. (2.9)).

A few optimization opportunities present themselves in the code below, namely, since most of the time-complexity comes from repeated evaluations of v_{ijkl} in the loops, a good first step is to attempt to parallelize these for-loops using suitable OpenMP pragmas. However this is not entirely straightforward since for most loops, the index of the inner loop strictly depends on the index of the outer, resulting in a significantly worse load distribution over the available threads. An effective solution to this problem is to *fuse* the nested loops by hand, for instance instead of looping over $m \in [1, M)$ and $n \in [m, M)$ in a nested fashion, a new index $k \in [0, M(M-1)/2)$ is introduced alongside a suitable mapping $k \mapsto (m, n)$ to compute the old indices. As a consequence, each problematic nested loops in our code may be expressed as a single loop yielding better load distribution, in this project alone a 200% increase in performance was seen by utilizing this method.

Algorithm 1: Rayleigh-Schrödinger perturbation theory applied to the one-component Gross-Pitaevskii equation

Input : Set of eigenstates and eigenenergies $\{|\phi_i\rangle\}$, $\{\mu_i\}$, $i \in [0, M-1]$ that solve Eq. (2.14).
Output: Ground state energy E calculated using RSPT up to order three.

// Compute zeroth and first order energy shift
$E_0 \leftarrow N\mu_0$
$E_1 \leftarrow -\frac{1}{2}gN(N-1)v_{0000}$
// Compute second order energy shift
$E_2 \leftarrow 0$
$t = []$// Fixed size array indexed by (i,j)
for $m \leftarrow 1$ **to** M **do**
  for $n \leftarrow m$ **to** M **do**
    $me \leftarrow \left\{1 + (\frac{1}{\sqrt{2}} - 1)\delta_{m,n}\right\} g\sqrt{N(N-1)}v_{mn00}$
    $\Delta E \leftarrow 2\mu_0 - \mu_m - \mu_n$
    $t[m,n] \leftarrow me/\Delta E$
    $E_2 \leftarrow E_2 + me \times me/\Delta E$
// Compute third order energy shift. Starting with contributions from integrals v_{0000}
$E_{0000} \leftarrow 0$
for $m \leftarrow 1$ **to** M **do**
  for $n \leftarrow m$ **to** M **do**
    $E_{0000} \leftarrow E_{0000} + t[m,n]^2$
$E_{0000} \leftarrow E_{0000} v_{0000}$
// Next, contributions from v_{m0n0}
$E_{m0n0} \leftarrow 0$
for $m \leftarrow 1$ **to** M **do**
  for $n \leftarrow 1$ **to** M **do**
    $sum \leftarrow 0$
    for $p \leftarrow 1$ **to** M **do**
      $sum \leftarrow sum + t[m,p]t[n,p]\left\{1 + (\sqrt{2}-2)(\delta_{m,p} + \delta_{n,p}) + (3 - 2\sqrt{2})\delta_{m,p}\delta_{n,p}\right\}$
    $E_{m0n0} \leftarrow E_{m0n0} + gv_{m0n0} \times sum$
$E_{m0n0} \leftarrow E_{m0n0}(N-3)$
// Lastly, contributions from v_{mnpq}
$E_{mnpq} \leftarrow 0$
for $m \leftarrow 1$ **to** M **do**
  for $n \leftarrow m$ **to** M **do**
    for $p \leftarrow 1$ **to** M **do**
      for $q \leftarrow p$ **to** M **do**
        $E_{mnpq} \leftarrow$
        $E_{mnpq} + gv_{mnpq}t[m,n]t[p,q]\left\{2 + (\sqrt{2}-2)(\delta_{mn} + \delta_{pq}) + (3 - 2\sqrt{2})\delta_{mn}\delta_{pq}\right\}$
// We can now return the new energy
return $E_0 + E_1 + E_2 + (E_{0000} + E_{m0n0} + E_{mnpq})$

Appendix D

Derivation of the integral over the product of four wave functions in the harmonic oscillator basis

Provided wave functions $\phi_n(x) = \sum_n c_n \chi_n(x)$ expressed in the harmonic oscillator basis $\chi_n(x) = \frac{1}{\sqrt{2^n n!}} \left(\frac{\omega}{\pi}\right)^{1/4} e^{-\omega x^2/2} H_n(\omega x)$ where H_n are the Hermite polynomials, the integral Eq. (2.9) may be expanded as

$$\begin{aligned} v_{ijkl} &= \int_{-\infty}^{\infty} \mathrm{d}x\, \phi_i(x)\phi_j(x)\phi_k(x)\phi_l(x) \\ &= \int_{-\infty}^{\infty} \mathrm{d}x\, \left(\sum_i c_i\chi_i(x)\right)\left(\sum_j d_j\chi_j(x)\right)\left(\sum_j e_k\chi_k(x)\right)\left(\sum_k f_l\chi_l(x)\right) \\ &= \int_{-\infty}^{\infty} \mathrm{d}x \sum_{ijkl} c_i d_j e_k f_l \chi_i(x)\chi_j(x)\chi_k(x)\chi_l(x), \end{aligned} \tag{D.1}$$

then swapping the order of integration and summation as well as expanding the basis functions yields

$$\begin{aligned} v_{ijkl} = \sum_{ijkl} \overbrace{c_i d_j e_k f_l \left[\frac{\omega}{\pi} \times \frac{1}{\sqrt{2^{i+j+k+l} i!j!k!l!}}\right]}^{K_{ijkl}} \\ \times \int_{-\infty}^{\infty} \mathrm{d}x\, e^{-2\omega x^2} H_i(\sqrt{\omega}x) H_j(\sqrt{\omega}x) H_k(\sqrt{\omega}x) H_l(\sqrt{\omega}x), \end{aligned} \tag{D.2}$$

where K_{ijkl} represents a grouping of coefficients to save space. Focusing on the last integral and introducing the substitution $u := \sqrt{\omega}x \Rightarrow \mathrm{d}x = \frac{1}{\sqrt{\omega}}\mathrm{d}u$ results in

$$v_{ijkl} = \frac{1}{\sqrt{\omega}} \sum_{ijkl} K_{ijkl} \int_{-\infty}^{\infty} \mathrm{d}u\, e^{-2u^2} H_i(u) H_j(u) H_k(u) H_l(u), \tag{D.3}$$

and at this point some external results are necessary to proceed. Specifically the evaluation of the integral

$$\begin{aligned} &h(i,j,k) \\ &\quad = \int_{-\infty}^{\infty} \mathrm{d}u\, e^{-2u^2} H_i(u) H_j(u) H_k(u) \\ &\quad = \sqrt{\frac{\pi}{2}} \begin{cases} (i+j-k-1)!!(i-j+k-1)!!(-i+j+k-1)!!, i+j+k \ \textit{even}; \\ 0, \quad \textit{otherwise} \end{cases} \end{aligned} \tag{D.4}$$

provided by Ref. [61], where $n!! = n(n-2)!!$ refers to the *double* factorial, behaving similarly to the regular $n!$ however only including numbers of the same parity as n. Moreover extending $n!!$ to odd negative integers is necessary resulting in $n!! = \frac{(n+2)!!}{n+2}$, where n is negative and odd, this follows directly from solving for $(n-2)!!$ in $n!! = n(n-2)!!$ and relabeling $n \to (n-2)$.

In addition to Eq. (D.4), Theorem 6.8.1 from Ref. [62] which states that the product of two Hermite polynomials $H_i(x)$ and $H_j(x)$ may be calculated as

$$H_i(x) H_j(x) = \sum_{m=0}^{\min(i,j)} \binom{i}{m} \binom{j}{m} 2^m m! H_{i+j-2m}(x), \tag{D.5}$$

is also needed. Getting back to where we left of regarding Eq. (D.3) and applying Eq. (D.5) gives

$$\begin{aligned} v_{ijkl} &= \frac{1}{\sqrt{\omega}} \sum_{ijkl} K_{ijkl} \int_{-\infty}^{\infty} \mathrm{d}u\, e^{-2u^2} H_i(u) H_j(u) H_k(u) H_l(u) \\ &= \frac{1}{\sqrt{\omega}} \sum_{ijkl} K_{ijkl} \sum_{m=0}^{\min(i,j)} \binom{i}{m} \binom{j}{m} 2^m m! \int_{-\infty}^{\infty} \mathrm{d}u\, e^{-2u^2} H_{i+j-2m}(u) H_k(u) H_l(u), \end{aligned} \tag{D.6}$$

and lastly applying Eq. (D.4) to the above results in

$$v_{ijkl} = \frac{1}{\sqrt{\omega}} \sum_{ijkl} K_{ijkl} \sum_{m=0}^{\min(i,j)} \binom{i}{m} \binom{j}{m} 2^m m! h(i+j-2m, k, l) \tag{D.7}$$

where $h(i+j-2m,k,l)$ is only non-zero when $i+j+k+l$ is even, greatly reducing the number of summations, on top of this, expanding K_{ijkl}, $h(i,j,k)$ and the binomial

coefficients gives

$$
\begin{aligned}
v_{ijkl} = \frac{1}{\sqrt{\omega}} \sum_{\substack{ijkl,\\ i+j+k+l \text{ even}}} (c_i d_j e_k f_l) \left[\frac{\omega}{\pi} \times \frac{1}{\sqrt{2^{i+j+k+l} i!j!k!l!}} \right] \\
\times \sum_{m=0}^{\min(i,j)} \left[\frac{i!}{(i-m)!m!} \times \frac{j!}{(j-m)!m!} \right] 2^m m! \\
\times \sqrt{\frac{\pi}{2}} [(i+j-2m)+k-l-1]!! \times [(i+j-2m)-k+l-1]!! \\
\times [-(i+j-2m)+k+l-1]!!
\end{aligned}
\tag{D.8}
$$

$$
\begin{aligned}
= \sqrt{\frac{\omega}{2\pi}} \sum_{\substack{ijkl,\\ i+j+k+l \text{ even}}} (c_i d_j e_k f_l) \frac{\sqrt{(i!j!)/(k!l!)}}{2^{(i+j+k+l)/2}} \sum_{m=0}^{\min(i,j)} \left[\frac{2^m}{(i-m)!(j-m)!m!} \right] \\
\times [(i+j-2m)+k-l-1]!! \times [(i+j-2m)-k+l-1]!! \\
\times [-(i+j-2m)+k+l-1]!!,
\end{aligned}
$$

further simplifications are without a doubt possible, put this is as far as we go for this derivation. Reason being, that for all practical purposes most of the above may be pre-computed and looked up at runtime, effectively reducing the equation to

$$
v_{ijkl} = \sum_{\substack{ijkl,\\ i+j+k+l \text{ even}}} c_i d_j e_k f_l \times \text{cache}(i,j,k,l), \tag{D.9}
$$

where $\text{cache}(i,j,k,l)$ represent a cache lookup. Then of course more stress is put on the caching method of choice, but that is beside the point.

Bibliography

[1] Lev Pitaevskii and Sandro Stringari, *Bose-Einstein Condensation.* Clarendon Street, Oxford: Oxford University Press, 2003.

[2] K. B. Davis, M. O. Mewes, M. R. Andrews, N. J. van Druten, D. S. Durfee, D. M. Kurn, and W. Ketterle, "Bose-einstein condensation in a gas of sodium atoms," *Phys. Rev. Lett.*, vol. 75, pp. 3969–3973, Nov 1995.

[3] M. H. Anderson, J. R. Ensher, M. R. Matthews, C. E. Wieman, and E. A. Cornell, "Observation of bose-einstein condensation in a dilute atomic vapor," *Science*, vol. 269, no. 5221, pp. 198–201, 1995.

[4] R. Wynar, R. Freeland, D. Han, C. Ryu, and D. Heinzen, "Molecules in a bose-einstein condensate," *Science*, vol. 287, no. 5455, pp. 1016–1019, 2000.

[5] M. Greiner, C. A. Regal, and D. S. Jin, "Emergence of a molecular bose–einstein condensate from a fermi gas," *Nature*, vol. 426, no. 6966, pp. 537–540, 2003.

[6] Z. Zhang, L. Chen, K. Yao, and C. Chin, "Atomic bose-einstein condensate to molecular bose-einstein condensate transition," *arXiv preprint arXiv:2006.15297*, 2020.

[7] J. Keeling and S. Kéna-Cohen, "Bose–einstein condensation of exciton-polaritons in organic microcavities," *Annual review of physical chemistry*, vol. 71, pp. 435–459, 2020.

[8] A. Zvyagin, "Redistribution (condensation) of magnons in a ferromagnet under pumping," *Low Temperature Physics*, vol. 33, no. 11, pp. 948–951, 2007.

[9] T. Damm, J. Schmitt, Q. Liang, D. Dung, F. Vewinger, M. Weitz, and J. Klaers, "Calorimetry of a bose–einstein-condensed photon gas," *Nature communications*, vol. 7, no. 1, pp. 1–5, 2016.

[10] J. Klaers, J. Schmitt, F. Vewinger, and M. Weitz, "Bose–einstein condensation of photons in an optical microcavity," *Nature*, vol. 468, no. 7323, pp. 545–548, 2010.

[11] E. K. U. Gross, E. Runge, and O. Heinonen, *Many-Particle Theory.* Adam Hilger, 1991.

[12] C.J. Pethick and H. Smith, *Bose-Einstein condensation in dilute gases.* Cambridge University Press, 2002.

[13] G. Baym and C. Pethick, "Ground-state properties of magnetically trapped bose-condensed rubidium gas," *Physical review letters*, vol. 76, no. 1, p. 6, 1996.

[14] M. Edwards, P. Ruprecht, K. Burnett, R. Dodd, and C. W. Clark, "Collective excitations of atomic bose-einstein condensates," *Physical review letters*, vol. 77, no. 9, p. 1671, 1996.

[15] D. Hutchinson, E. Zaremba, and A. Griffin, "Finite temperature excitations of a trapped bose gas," *Physical review letters*, vol. 78, no. 10, p. 1842, 1997.

[16] D. Jin, J. Ensher, M. Matthews, C. Wieman, and E. A. Cornell, "Collective excitations of a bose-einstein condensate in a dilute gas," *Physical review letters*, vol. 77, no. 3, p. 420, 1996.

[17] D. Rokhsar, "Vortex stability and persistent currents in trapped bose gases," *Physical review letters*, vol. 79, no. 12, p. 2164, 1997.

[18] R. Dum, J. Cirac, M. Lewenstein, and P. Zoller, "Creation of dark solitons and vortices in bose-einstein condensates," *Physical Review Letters*, vol. 80, no. 14, p. 2972, 1998.

[19] P. Fedichev and G. Shlyapnikov, "Dissipative dynamics of a vortex state in a trapped bose-condensed gas," *Physical Review A*, vol. 60, no. 3, p. R1779, 1999.

[20] M. R. Matthews, B. P. Anderson, P. Haljan, D. Hall, C. Wieman, and E. A. Cornell, "Vortices in a bose-einstein condensate," *Physical Review Letters*, vol. 83, no. 13, p. 2498, 1999.

[21] C. Raman, J. Abo-Shaeer, J. Vogels, K. Xu, and W. Ketterle, "Vortex nucleation in a stirred bose-einstein condensate," *Physical review letters*, vol. 87, no. 21, p. 210402, 2001.

[22] J. Abo-Shaeer, C. Raman, J. Vogels, and W. Ketterle, "Observation of vortex lattices in bose-einstein condensates," *Science*, vol. 292, no. 5516, pp. 476–479, 2001.

[23] D. S. Petrov, "Quantum mechanical stabilization of a collapsing bose-bose mixture," *Phys. Rev. Lett.*, vol. 115, p. 155302, Oct 2015.

[24] G. Semeghini, G. Ferioli, L. Masi, C. Mazzinghi, L. Wolswijk, F. Minardi, M. Modugno, G. Modugno, M. Inguscio, and M. Fattori, "Self-bound quantum droplets of atomic mixtures in free space," *Phys. Rev. Lett.*, vol. 120, p. 235301, Jun 2018.

[25] L.S. Cederbaum and A.I. Streltsov, "Best mean-field for condensates.," *Physics Letters A*, vol. 318, no. 6, pp. 564 – 569, 2003.

[26] M. Kot, *A First Course in the Calculus of Variations*. American Mathematical Society, 2014.

[27] D. Cremer, "From configuration interaction to coupled cluster theory: The quadratic configuration interaction approach," *WIREs Computational Molecular Science*, vol. 3, no. 5, pp. 482–503, 2013.

[28] R. J. Bartlett, "Many-body perturbation theory and coupled cluster theory for electron correlation in molecules," *Annual Review of Physical Chemistry*, vol. 32, no. 1, pp. 359–401, 1981.

[29] A. Tichai, P. Arthuis, T. Duguet, H. Hergert, V. Somá, and R. Roth, "Bogoliubov many-body perturbation theory for open-shell nuclei," *Physics Letters B*, vol. 786, pp. 195–200, 2018.

[30] P. Demol, M. Frosini, A. Tichai, V. Somà, and T. Duguet, "Bogoliubov many-body perturbation theory under constraint," *Annals of Physics*, vol. 424, p. 168358, 2021.

[31] A. Signoracci, T. Duguet, G. Hagen, and G. Jansen, "Ab initio bogoliubov coupled cluster theory for open-shell nuclei," *Physical Review C*, vol. 91, no. 6, p. 064320, 2015.

[32] C. Møller and M. S. Plesset, "Note on an approximation treatment for many-electron systems," *Physical review*, vol. 46, no. 7, p. 618, 1934.

[33] U. Bozkaya, J. M. Turney, Y. Yamaguchi, H. F. Schaefer III, and C. D. Sherrill, "Quadratically convergent algorithm for orbital optimization in the orbital-optimized coupled-cluster doubles method and in orbital-optimized second-order møller-plesset perturbation theory," *The Journal of chemical physics*, vol. 135, no. 10, p. 104103, 2011.

[34] H. Pathak, T. Sato, and K. L. Ishikawa, "Study of laser-driven multielectron dynamics of ne atom using time-dependent optimised second-order many-body perturbation theory," *Molecular Physics*, vol. 118, no. 21-22, p. e1813910, 2020.

[35] D. Dast, D. Haag, H. Cartarius, J. Main, and G. Wunner, "Eigenvalue structure of a bose–einstein condensate in a-symmetric double well," *Journal of Physics A: Mathematical and Theoretical*, vol. 46, no. 37, p. 375301, 2013.

[36] J. A. Pople, M. Head-Gordon, and K. Raghavachari, "Quadratic configuration interaction. a general technique for determining electron correlation energies," *The Journal of Chemical Physics*, vol. 87, no. 10, pp. 5968–5975, 1987.

[37] J. J. Sakurai and Jim Napolitano, *Modern Quantum Mechanics*. Cambridge University Press, 2 ed., 2017.

[38] M. Lewin, "Mean-field limit of bose systems: rigorous results," 2015.

[39] E. J. Mueller, T.-L. Ho, M. Ueda, and G. Baym, "Fragmentation of bose-einstein condensates," *Physical Review A*, vol. 74, no. 3, p. 033612, 2006.

[40] O. Elgarøy and C. J. Pethick, "Absence of fragmentation of the condensate in a model for bosons in a trap," *Phys. Rev. A*, vol. 59, pp. 1711–1714, Feb 1999.

[41] C. C. J. Roothaan, "New developments in molecular orbital theory," *Rev. Mod. Phys.*, vol. 23, pp. 69–89, Apr 1951.

[42] D. R. Hartree, "The calculation of atomic structures," 1957.

[43] A. T. B. Gilbert, N. A. Besley, and P. M. W. Gill, "Self-consistent field calculations of excited states using the maximum overlap method (mom)," *The Journal of Physical Chemistry A*, vol. 112, no. 50, pp. 13164–13171, 2008. PMID: 18729344.

[44] H. B. Schlegel and J. McDouall, "Do you have scf stability and convergence problems?," in *Computational advances in organic chemistry: Molecular structure and reactivity*, pp. 167–185, Springer, 1991.

[45] A. Iserles, *A First Course in the Numerical Analysis of Differential Equations*. Cambridge Texts in Applied Mathematics, Cambridge University Press, 2 ed., 2008.

[46] P. S. Epstein, "The stark effect from the point of view of schroedinger's quantum theory," *Phys. Rev.*, vol. 28, pp. 695–710, Oct 1926.

[47] R. K. Nesbet, "Configuration interaction in orbital theories," *Proc. R. Soc. Lond.*, vol. 230, no. 1182, pp. 312–322, 1955.

[48] P. J. Davis, *Methods of Numerical Integration*. Academic Press, 2 ed., 1984. Ch. 2,3 & 4.

[49] Richard B. Lehoucq, Danny C. Sorensen, and Chao Yang, *ARPACK Users' Guide: Solution of Large-scale Eigenvalue Problems with Implicitly Restarted Arnoldi Methods*. Philadelphia: SIAM, 1998.

[50] "ARPACK-NG." Open source collaboration, started by the Debian, Octave, and Scilab projects, to keep to original ARPACK routines by Rice University up to date. Repository available at `https://github.com/opencollab/arpack-ng`.

[51] "OpenBLAS." Maintained by Zhang Xianyi, available at `https://openblas.net`.

[52] L. Dagum and R. Menon, "Openmp: an industry standard api for shared-memory programming," *IEEE computational science and engineering*, vol. 5, no. 1, pp. 46–55, 1998.

[53] J. Nickolls, I. Buck, M. Garland, and K. Skadron, "Scalable parallel programming with cuda: Is cuda the parallel programming model that application developers have been waiting for?," *Queue*, vol. 6, no. 2, pp. 40–53, 2008.

[54] X. Antoine and R. Duboscq, "Gpelab, a matlab toolbox to solve gross–pitaevskii equations i: Computation of stationary solutions," *Computer Physics Communications*, vol. 185, no. 11, pp. 2969 – 2991, 2014.

[55] P. Pulay, "Convergence acceleration of iterative sequences. the case of scf iteration," *Chemical Physics Letters*, vol. 73, no. 2, pp. 393 – 398, 1980.

[56] M. Albiez, R. Gati, J. Fölling, S. Hunsmann, M. Cristiani, and M. K. Oberthaler, "Direct observation of tunneling and nonlinear self-trapping in a single bosonic josephson junction," *Physical review letters*, vol. 95, no. 1, p. 010402, 2005.

[57] G. Milburn, J. Corney, E. M. Wright, and D. Walls, "Quantum dynamics of an atomic bose-einstein condensate in a double-well potential," *Physical Review A*, vol. 55, no. 6, p. 4318, 1997.

[58] D. Petrov and G. Astrakharchik, "Ultradilute low-dimensional liquids," *Physical review letters*, vol. 117, no. 10, p. 100401, 2016.

[59] S. Attal, "Lecture 8, fock spaces." Accessed: 2021-02-21. Available at: `http://math.univ-lyon1.fr/~attal/Fock_Spaces.pdf`.

[60] A. Beggi, I. Siloi, C. Benedetti, E. Piccinini, L. Razzoli, P. Bordone, and M. G. Paris, "Back and forth from fock space to hilbert space: a guide for commuters," *European Journal of Physics*, vol. 39, no. 6, p. 065401, 2018.

[61] A. Minakov, "Question about integral of product of four hermite polynomials integrated with squared weight," *arXiv preprint arXiv:1911.03942*, 2019.

[62] G. E. Andrews, R. Askey, and R. Roy, *Special functions*. No. 71, Cambridge university press, 1999.